Joule Centre Research Grant Joint Final Report
(Lancaster University and Manchester Metropolitan University)

Announced Start Date: 1st January 2008

Announced End Date: 30th June 2009

Title: A Joint Numerical and Experimental Study of a Surging Point Absorbing Wave Energy Converter (WRASPA)

Joule Grant No: JIRP306/02

Principal Investigator – Lancaster University: Eur Ing George A Aggidis

Principal Investigator – Manchester Metropolitan University: Prof Clive Mingham

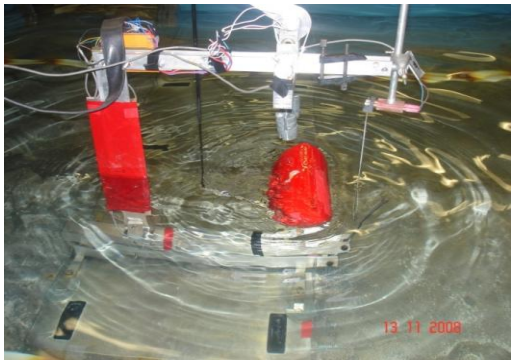

WRASPA in experimental wave tank

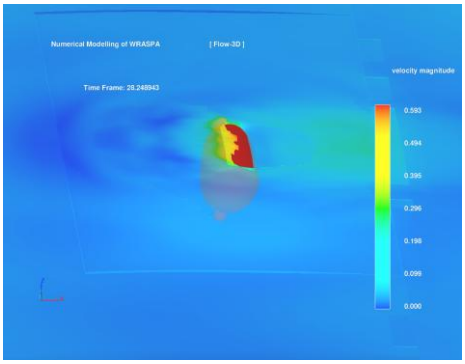

WRASPA in numerical wave tank

Contents

1. Introduction

There is growing acceptance both within the UK and overseas that all possible alternative sources of energy that do not produce greenhouse gases, should be developed and exploited. The power in sea waves is a very large renewable global resource. The UK has the greatest wave-power resource of any country in Europe; it is thus uniquely positioned to benefit from wave-power technology. Such technology would bring further economic benefit by exporting wave-power technology and devices.
A wide variety of wave power devices has been proposed, both in the UK and elsewhere. Some have been developed to full-size prototype stage and it might be expected that some clear indications would have appeared by now about the form that wave energy converters (WECs) are likely to take. However, thus far, this has not happened, and it is not clear that any of the devices so far developed or proposed will be able to capture energy economically.

Following the Kyoto agreement of 1997, national governments have set targets for the proportion of electricity to be generated from renewable resources. In the UK, for example, 10% of electricity generation must come from renewable sources by 2010 compared with 3.5% generated from renewable sources in 2000. The situation differs throughout the UK, and for instance, Scotland is aiming at 18% by 2010. Around three quarters of all sun-derived energy on the earth is received by the oceans and seas and, according to the World Energy Council, the oceans could supply twice as much energy as the world now consumes. Although significant advances have been recently made in the design of efficient wave energy converters, there is still a great potential for further development. Ideally, the industry needs a range of devices suitable for operating in a variety of weather, geomorphic, and hydrodynamic conditions. The main goal of this research is to help in achieving this target by creating scientific and technical foundation for a largely overlooked class of wave energy converters that, on the basis of preliminary studies, have very good economic potential.

The WRASPA* Concept (*Wave-driven, Resonant, Arcuate-action, Surging Point-Absorber) was invented at LU in 2006 following a series of laboratory tests on resonant collectors moving purely in surge. Unlike other sea bed mounted WECs (e.g. Frond, Waveroller, Oyster and BioWave) WRASPA is effectively resonant in surge and tests have shown capture ratios exceeding unity.

The concept has been evaluated and developed by means of computer modelling (forming part 3 of this report) and wave-tank tests (part 2 of the report) in a joint program between Manchester Metropolitan University (MMU) and Lancaster University (LU).

In the concept, wave forces act on the face of a collector body carried on an arm that rotates about a fixed horizontal axis some 20m below sea level so that the body is resonant at about the frequency of the ocean swell. The varying input power is extracted at the pivot by a power take-off (PTO) system that modulates the output power to match the input. The output is ‘smoothed’ using an on-board control system incorporating a short-term energy store so that it can then be used to generate steady electrical power that

will be transmitted by cable along the sea bed.

It is envisaged that, once the design is optimised, full-sized converters weighing about 400t each (un-ballasted) would be manufactured on land, then moved to site by a specialist handling vessel and inserted into pre-installed piles that would protrude above the sea bed in water depths of about 25m. During the deployment process ballast weights would be added to the collector arm, at or near the main pivot, to counter the buoyancy force acting on the collector body. When working the collectors would be driven to face the prevailing wave direction and move to and fro in the direction of wave travel. They would do this in response to inputs from local sensors that would measure the direction, strength and frequency of the energy carrying parts of the prevailing wave spectrum.

The PIs of this joint research project would like to acknowledge the support of the Joule Centre and NWDA for funding this research and the Universities of Manchester (MU) and Edinburgh (EU) for allowing the WRASPA researchers to use their respective wave tanks in order to carry out additional comparative experimental modelling.

Background

The evolution of WRASPA followed a series of experiments in 2006 [2.1] in which a surge-resonant collector was carried on an apparatus comprising a frictionless carriage moving on a
fixed horizontal rail with its movements centred by long steel springs. With this it was possible to find Capture Ratios greater than unity and, at resonance, amplitudes of motion were large, typically 4 or 5x the wave amplitude when working at maximum power. These results appeared to agree with the findings of Evans [2.2] and others for point absorbers moving in surge and clearly there was potential in finding a more practical version of this device. Thus, WRASPA was proposed as a bottom-hinged WEC with a relatively short pendulum length such that its pitching-surge motion was resonant with the waves and, as the angular movement of the collector body would be relatively small it could be said to be similar to the pure surge device, above, and would use the collector's own buoyancy as the restoring spring to make it resonant with the waves.

Trials with a semi-circular collector, streamlined by radiussing its edges showed promising performance [2.3] and it was clear, also, that this WEC's ability to survive storm waves was good.

At that stage, in a series of discussions between LU & MMU it was agreed that the design could benefit from a parallel study of the wave-collector interface in this device and that the results of such a study might be applicable more widely so the decision was taken to apply jointly to the Joule Centre for the funding that has supported the work described below. An impression of the full-scale design is seen in Fig.1.1

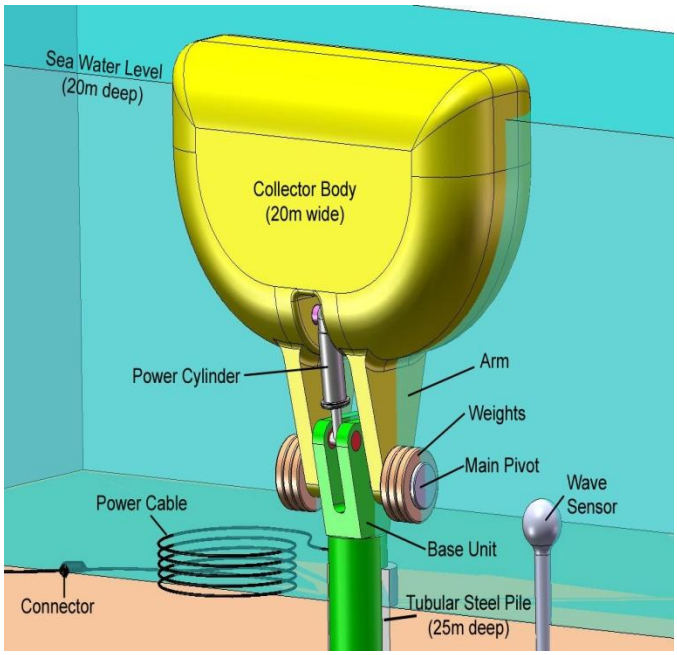

Reaction means

In order to extract power from a collector surface or body there must a relative motion between the collector and a reaction means and opposing forces acting on both such that work is done. In this case the reaction is provided by the seabed, via the pile and the "Base Unit". Because the collector is moving slowly, for example for a pitching-surge device at resonance with amplitude 0.25 rad at a period of 10sec the velocity would be 0.1 rad/s and to transfer say 1MW of power would require an average moment of 10MNm (or 1000 tm). Although this was seen as a major design issue for this class of device [2.4] it was indicated from [2.3] that peak forces would be well understood and as such could be allowed for - albeit at some cost.

1.1 Symbols & formulae

The actions of wave energy converters are normally described with reference to a 6 'degrees of freedom reference system where:-

Axis 1 represents surge, 2 sway and 3 heave with 4 being roll, 5, pitch and 6 yaw. Axis 1 (x) is aligned with the principal direction of wave propagation and axis 5 (y) is normal to axis 1 and horizontal. In a surge device the collector surface is essentially normal to axis 1 and translates along that axis.

In this pitching-surge WEC a fixed pivot axis, offset downwards from the collector's centre of effort, allows the collector's centre to move in both in pitch and in surge. The wave's energy may be passed into the collector via a pitch-damping system, for example a hydraulic circuit. The direct surge force and the slight variation in pressure amplitude with depth will both contribute to torque: both actions are accounted for if we integrate wave pressures and express them as a force vector acting at a point some distance from the pivot axis.

Symbols (See also Fig.2.36)

h = deviation of water level from UWL, m

h_{rms} = root mean square deviation from the sample mean,

$\dot{h}$ = surface elevation, m

(p-q) = lever arm from pivot to centre of pressure, m

θ = Collector pitch angle, rad

a_{55} = sum of added inertia and collector inertia kgm^2

b_{55} = radiation coeff. – Nms / rad
c_{55} = pitch stiffness of collector Nm/rad
d_{55} = an assumed drag factor referred to the pivot as a torque Nms^2/rad^2
I_Q = the 'dry' moment of inertia and consists of the product of a,

Λ = Damping constant of PTO Nms/rad

F_1= force coefficient Nm^{-1} (N per metre of wave elevation)

m_0= root mean square surface elevation, m

Some formulae used:-
Significant wave height $H_s = m_0 \times 4 = h_{rms} \times 4$

Wave power $P = 7658 \times Te \times (h_{rms})^2$ W/m
(NB the ratio 0.875 was used for T_e/T_p in Bretschneider spectra)

2. Experimentation

2.1 Methods

2.1.1 Apparatus

This is shown in Fig.2.1. A lever, connected to the collector body, under water, drives a light vertical pushrod acting on the top shaft via a crank, seen in the picture. This shaft mimics the rotation of the collector and is fitted with a motion sensor and two bi-directional band-brakes. The brakes can be instantaneously connected to the shaft by two solenoid-operated clutches. The frictional torque offered by brake 1 is half that of brake 2 so that, by binary combinations 0+0, 1+0, 0+2 and 1+2, a series of 3 steps plus zero are selectable by the control program.

The pylon (also red), astern of the collector is streamlined in section and so is 'invisible" to the waves. It carries the top shaft and, also, ahead of the collector-body, a single wave probe. This probe measures the water surface elevation close to the collector's front face and provides an input to the controller. The controller, written in LabView allows the user to set 3 threshold voltages, and compares these with the wave probe output and sends logic signals to two solid-state relays controlling the brakes in a binary combination as described above. (see also Fig.2.8) The pylon and the collector's pivot are both mounted on a fore-and-aft running underwater beam that itself is carried on a parallel linkage controlled by a lead-screw such that the whole apparatus can be raised and lowered over a range of 100 mm to control the collector's free-board. Torque is measured by a 4-gauge bridge on the under-water lever (thus avoiding almost all parasitic torques) and the horizontal force at the pivot is measured by a similar bridge fitted to the short vertical pillar that supports the pivot. Fig.2.2 shows a typical lab set-up in the MU tank.

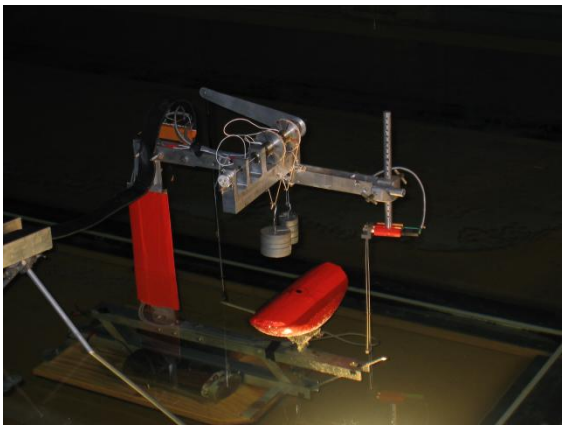

Fig. 2.1 The Mk II Rig viewed from the starboard bow and showing single wave probe ahead of collector's mid-point.

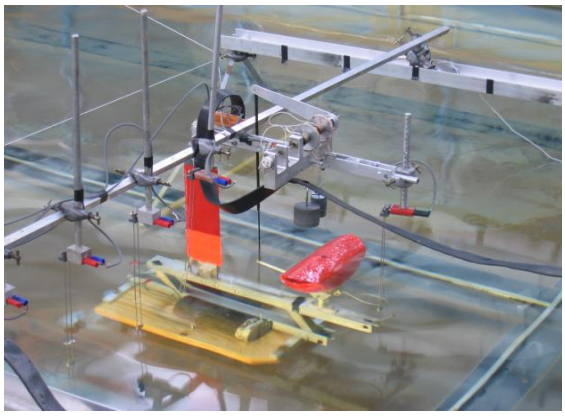

Fig.2.2 Apparatus in the Manchester University wave tank with moveable set of wave probes positioned astern of collector

2.1.2 Methods

The force and position transducers were calibrated before and after the test programme and wave gauges were calibrated daily. For power measurement, in general, the collector's freeboard was adjusted to set its natural frequency, ω_n equal to a desired value in relation to the waves (see Fig.2.4). This done, the "Max.Threshold" setting or other means was used to vary the average torque loading applied at the pivot. Power was then found from the linear or near-linear relation between torque and amplitude – see diagram in Fig.2.5

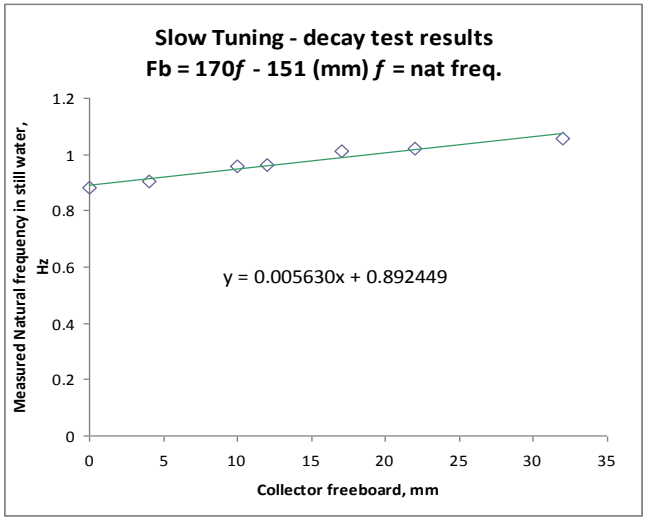

Fig. 2.4 Collector resonant frequency ω_n vs freeboard

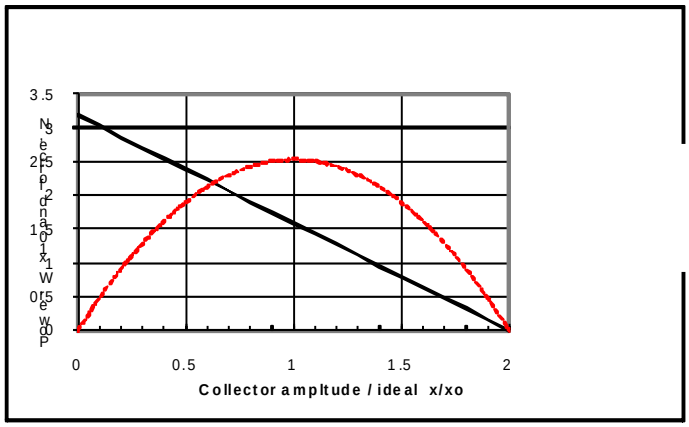

Fig. 2.5 showing derivation of power parabola from linear force/amplitude relationship.

2.1.3 Control aspects

Background and previous work

For WECs to extract power efficiently from waves their actions must ideally be matched to the incident waves. In effect a WEC is subject to two imperatives: the ever-changing wave force at its input and the steady voltage regime at the output. This whole topic is well covered in Salter et al [2.5] in which a wide range of PTO systems for wave power is considered.

The wave input to a WEC varies continuously and the sizes, periods and directions of particular components of a given sea state depend on the strengths, directions and durations of, sometimes distant, wind systems. These components, for simplicity, can be regarded as sine waves with differing amplitudes, periods and directions.

The annual data for a typical Hebridean site have be given by the Carbon Trust see Figs.

6 A,B,C and are expressed in terms of annual occurrences of waves of particular values of Hs and Te. Directional information is not included in these diagrams.

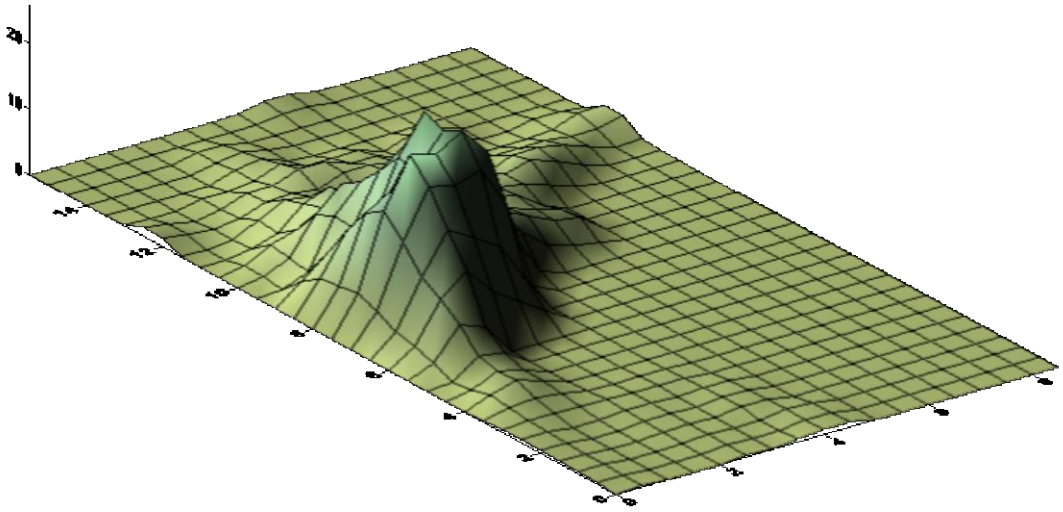

Fig.2.6A Carbon Trust's data set "Scatter data standard issue 1 - Medium" for 30 km offshore.

[LH axis = Te, sec RH axis = Hrms,m Vertical axis = annual occurrence.]

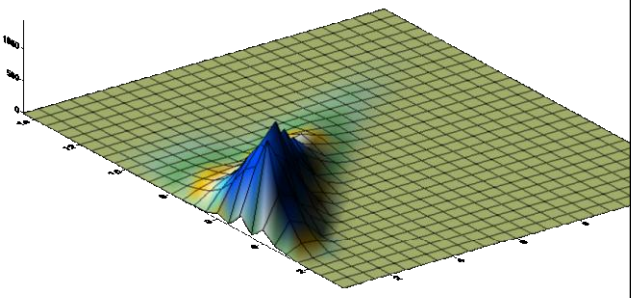

Fig.2.6B Carbon Trust's data set – Low" for 10 km offshore

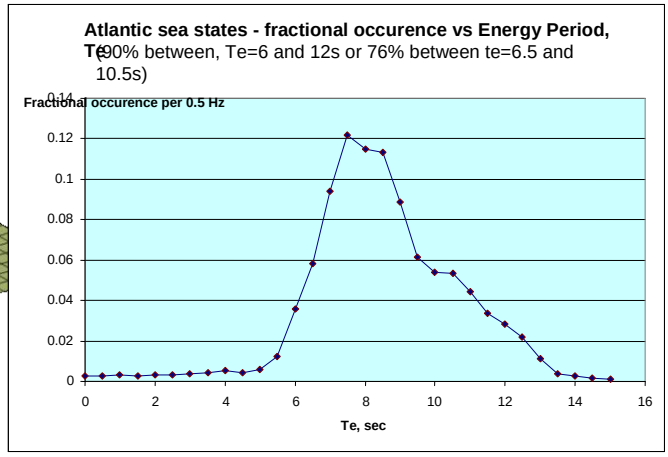

Fig.2.6C Carbon Trust's "Medium" summed to show main areas of interest

Slow Tuning.

From previous experiments in regular waves it was known that for maximum power capture the collector should be resonant with the wave. It was not known, in mixed seas,

which frequency to tune to and this was determined experimentally in tests – see below.

Control methods studied (see also reference [2.5])

1. Fixed force variable stroke.
This would be found in a hydraulic system with the outputs from a set of cylinders rectified and delivered to a – nominally fixed pressure - HP reservoir and thence to a turbine. This method was modelled in tests at Lancaster.

2. Stepwise Variable Damping.
(Note – this is similar to Salter et al's "Force proportional to velocity)
This concept was described at EWTEC 2007 [2.3] and in the proposal for the present project. A simplified hydraulic circuit for a full-scale device is shown in Fig 2.7. The intention is that the damping force should vary continuously so that at all times it would be kept at or near its ideal value – i.e.approx. 0.5 x the wave force. The best ratio would be found empirically and built into an algorithm that would control a set of directional control valves. For the 1/100 scale tank tests reported below, this method was implemented via the pair of computer-selectable small band brakes. Figure 2.8 shows the flowchart of the control system. Such a system could have either four or eight steps depending on whether the full-scale device had 2 or 4 double-acting cylinders.

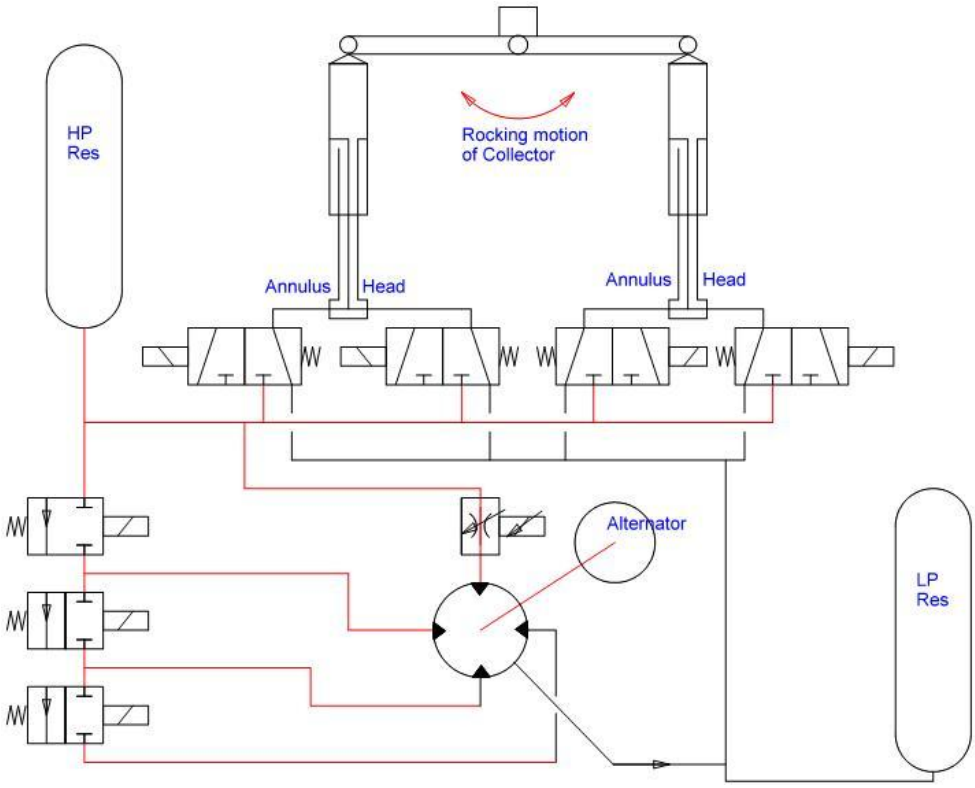

Fig 2.7 Simplified diagram of a possible Hydraulic circuit – 2 Cylinder version

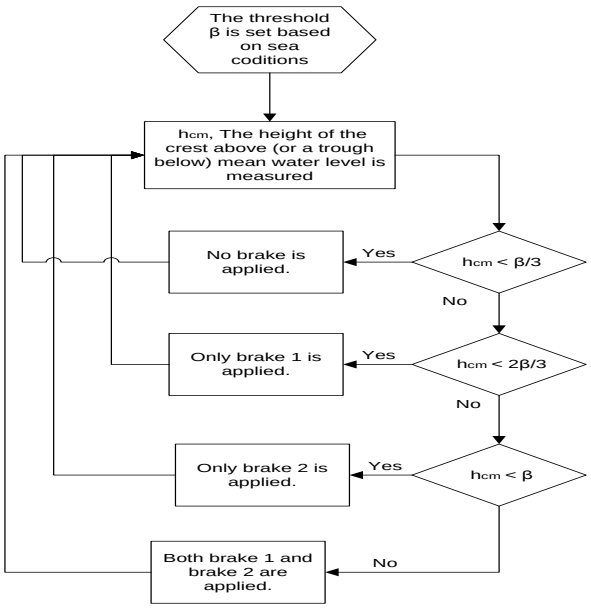

Figure 2.8: The control system flowchart

The input to the control system is the wave elevation at the collector's front face which was measured in the lab using a single wave probe. Fig.2.9 shows how the model system operated in practice with torques varying in response to brake signals.

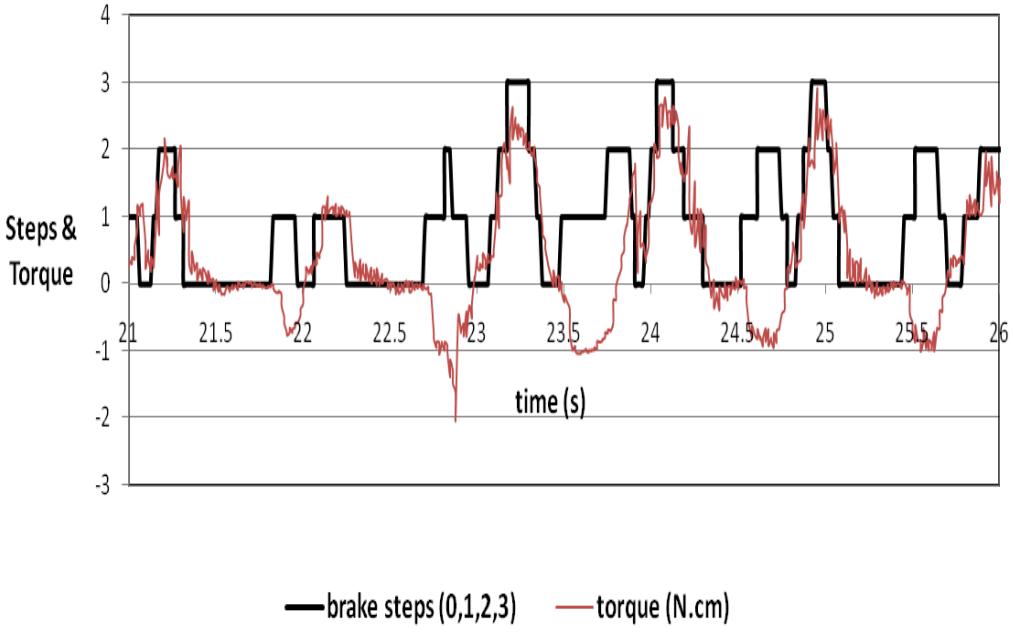

Figure 2.9: Typical record of torque vs. the brake steps

2.2 Results

2.2.1 Shape comparisons

This first stage of the work centred on finding collector shapes and sizes that were resonant at around 1 Hz and then to compare their potentials for capturing power. The 1 Hz frequency at 1/100 scale is equivalent to 0.I Hz (T=10s) at full scale and this is taken as being close to the best central frequency for a device with limited tuning ability to absorb the greatest proportion of the annual power spectrum in a N Atlantic site.

The 3 shapes and pivot depths found for ω_n close to 1Hz are seen in the table below and, by varying the freeboard we have seen how ω_n and power are changed. In the real device changing freeboard could be used as an effective tuning method. The 3 shapes have frontal areas of 0.026m^2 and volumes of almost 0.002m^3.

With the apparatus set-up with a particular shape the freeboard was adjusted to a chosen value. One or more decay tests were performed in still water for each shape and from the position trace the natural period was obtained (this proved to be very consistent for the duration of the trace as the oscillations decayed)

Collector shape			Un-damped		Fixed			
	Pivot depth, z_p	Freeboard, f_b	Collector amplitude, q_{cu}	Torque, T_{cu}	Torque, T_{cf}	Natural frequency (Hz)	Power, $P_{est.}$	Collector mass, m
	mm	mm	rad	Nm	Nm		W	Kg
Rhm2	174							0.138
		-20	0.12	0.012	0.194	.813	0.0164	
		0	0.34	0.023	0.294	1.0028	0.073	
		+20	0.32	0.022	0.231	0.96	0.069	
15^0 wedge	164							0.152
		-10	0.18	.01	0.173	0.830	0.020	
		0	0.31	0.0103	0.163	1.0027	0.0398	
		+10	0.372	0.0123	0.25	0.98	0.0375	
30^0 wedge	154							0.145
		-10	0.162	.0045	0.195	0.8134	0.023	
		0	0.305	0.0092	0.2349	0.9833	0.07	
		+10	0.381	0.0117	0.205	0.953	0.065	

Regular waves of this period were then passed down the tank and the collector motion (un-damped) was recorded. The collector was then locked and the same series of waves were passed down the tank while the collector torque and pivot force were measured. Results are summarised in Figs. 2.10 -2.15 below. The geometries are given in Figs.2.16 to 2.18

Conclusions.

1. The '"Mk2" rig was satisfactory in use. In particular the torque load when un-damped is low and the facility for raising and lowering the pivot position made for ease of experimentation.

2. All 3 shapes showed a rapid change in resonant frequency with freeboard as the collector was pulled down from just above UWL (+ve freeboard) to approx. 40 mm below.

3. Based on the results shown in graphs below the RHM2 shape was selected for future tests.

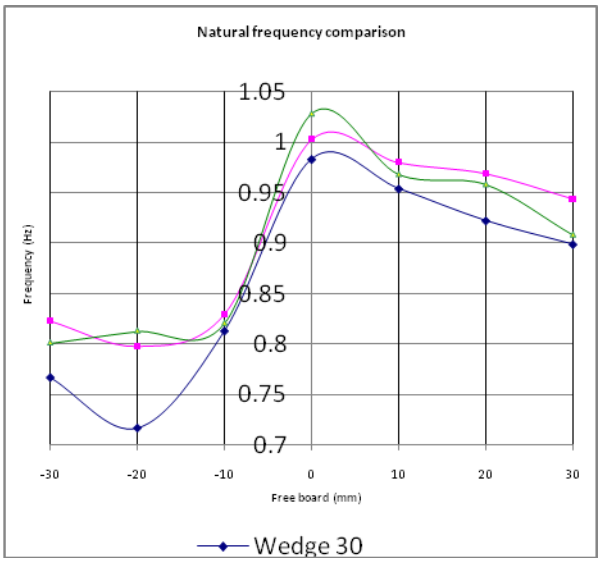

Figure 2.10: Comparison of natural frequency of the shapes

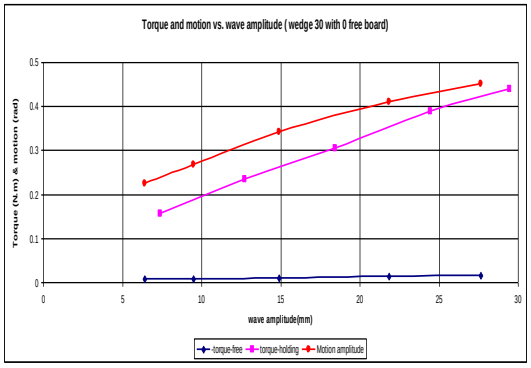

Figure 2.11: Torque and motion vs. wave amplitude for wedge 30 at 0 free board

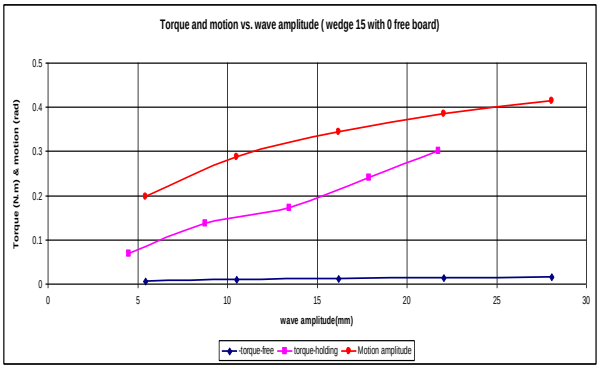

Figure 2.12: Torque and motion vs. wave amplitude for wedge 15 at 0 free-board

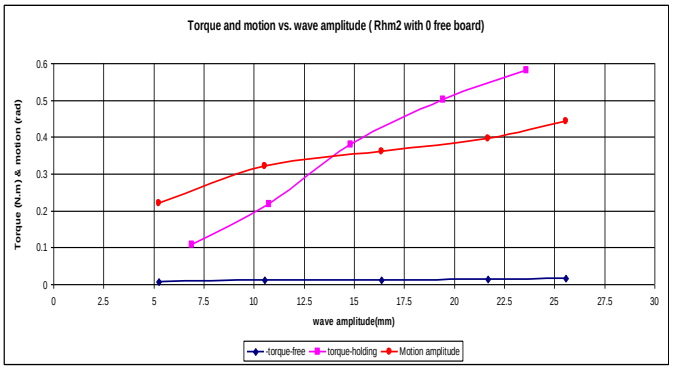

Figure 2.13: Torque and motion vs. wave amplitude for wedge RHM2 at 0 free-board

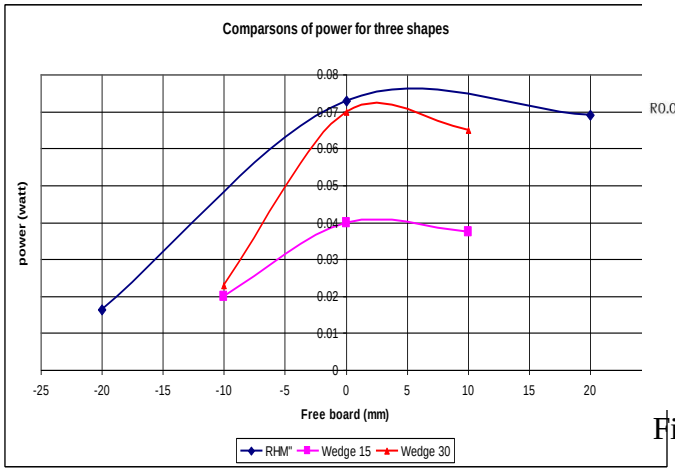

Figure 2.14: Comparison of peak power vs. free-board for three shapes

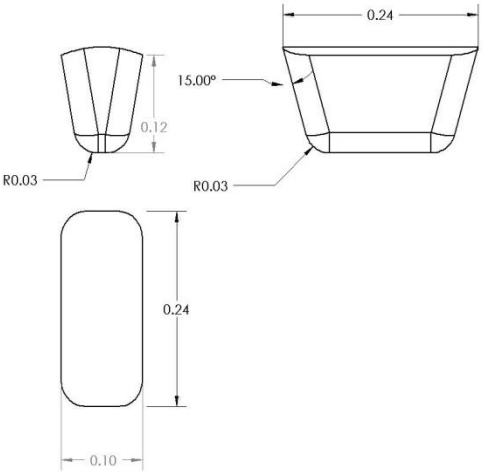

Figure 2.16: Wedge 15 geometry, in metres.

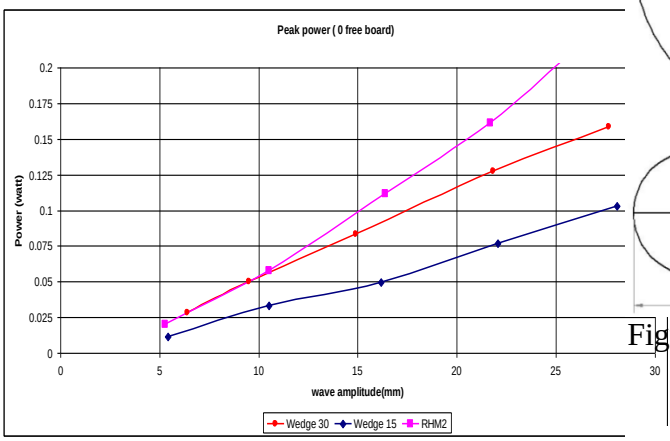

Figure 2.15: Comparison of peak power vs. wave amplitude for three shapes

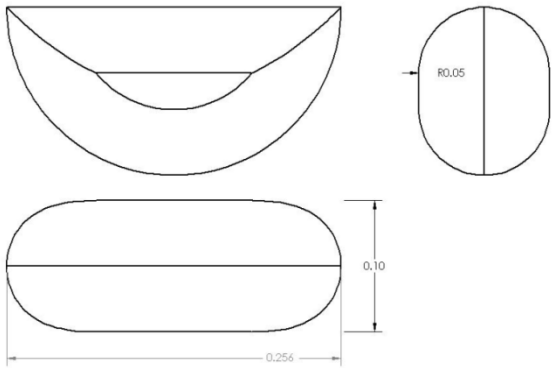

Figure 2.17: RHM2 Geometry, in metres

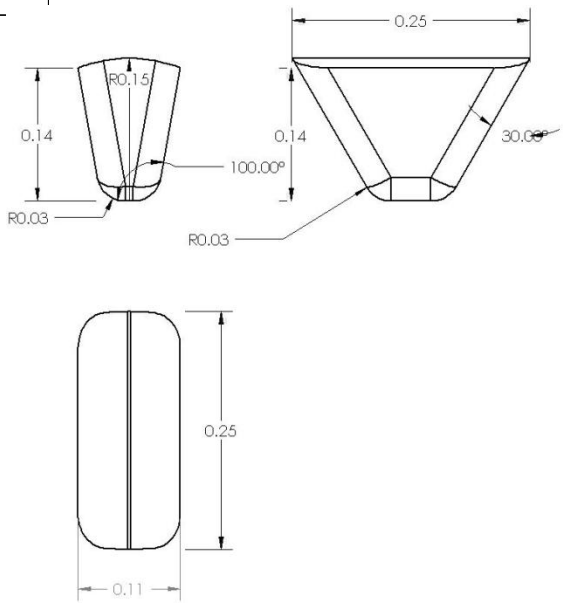

Figure 2.18: wedge 30 geometry, in metres

2.2.2 Regular waves – Edinburgh – with stepwise control

Most results are given in terms of Capture Width (CW), being Absorbed Power (Watts) / Incident Wave Power (Watts/metre)) so, in each case, model power can be found from the product of Incident wave power (x) x CW (y).

Results for regular waves – with the stepwise controller operating are shown in Fig.2.19. They show a clear trend of CW increasing in smaller waves. The curve shown was obtained indirectly by first plotting CW against 1/Power and obtaining a least-squares best fit line. The Point Absorber ideal CW of λ/π – in surge - is plotted on the Y axis, though not used in creating the curve, and fits well with the plotted line.

These results, scaled up, are shown in Fig.2.20 with absorbed power at 1 MW in waves of 90 kW/m and 0.5 MW in 30 Kw/m.

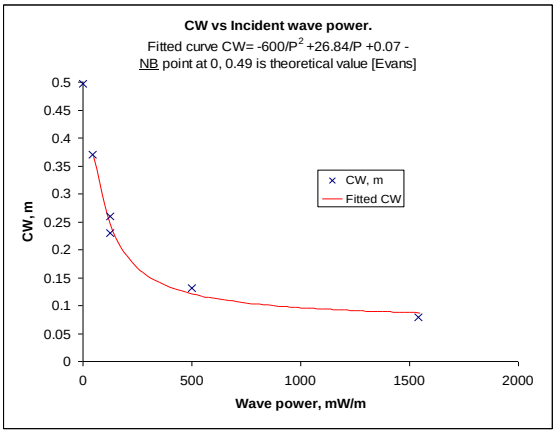

Fig.2.19 CW results in regular waves at T=1

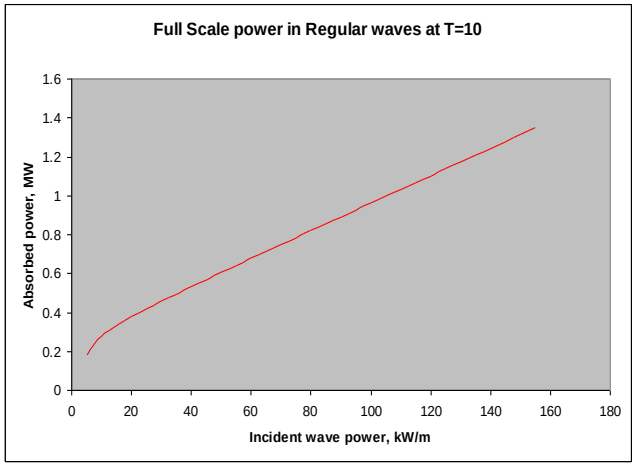

Fig.2.20 Results from Fig.2.19 scaled up

2.2.3 Mixed wave results

2D Mixed Waves – Tuning

In all the mixed seas tests at Manchester and at Edinburgh the stepwise controller was used. Before other tests were conducted the model was tested over a range of wave periods between Tp and Te and the max. power at each frequency was obtained. From these results the best compromise frequency was found - see Fig.2.21 below. For this typical wave condition it appears to lie at about 1.05 x fp for this model. (where fp=1/Tp) Subsequent testing was done with the model tuned "off" by this proportion from fp.

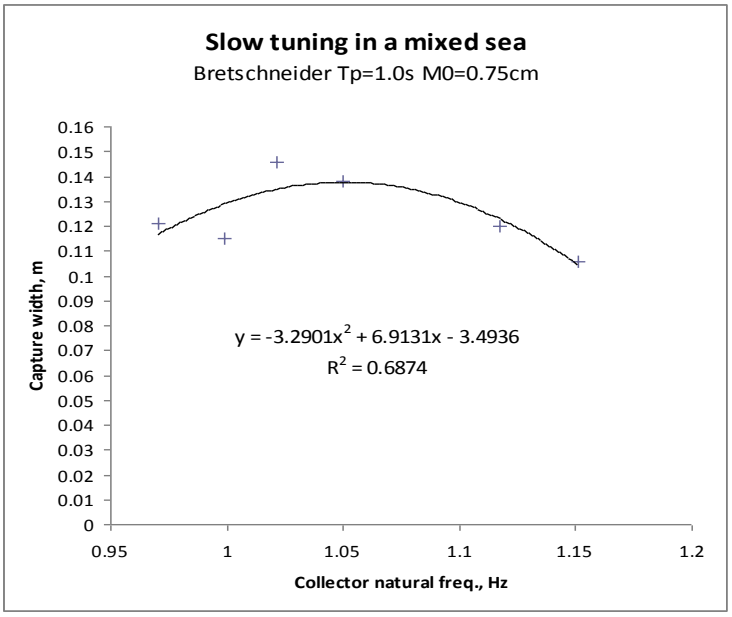

Fig.2.21 Slow tuning in mixed seas tests at Manchester University

Our main aim then, in these tests at MU and EU, was to assess how well the collector worked in mixed seas, with its relatively new stepwise controller – in Test 87, for example, shown in Fig.2.22, indicates how well the first stage of the control system works – switching between the 4 brake signal levels. Fig.2.23 shows for the same test, the torque varying in response to brake signals and both of these varying (albeit out of phase) with the incident wave recorded about 0.8m ahead of the collector. Fig.2.25 shows a section of time history from one test in mixed waves and the large difference between peak and average powers.

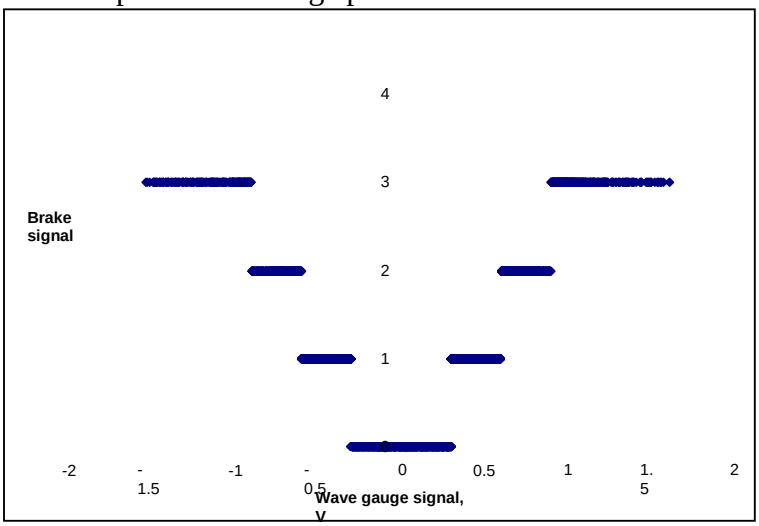

Fig. 2.22 Test 87 Brake signal vs wave height at collector face (V)

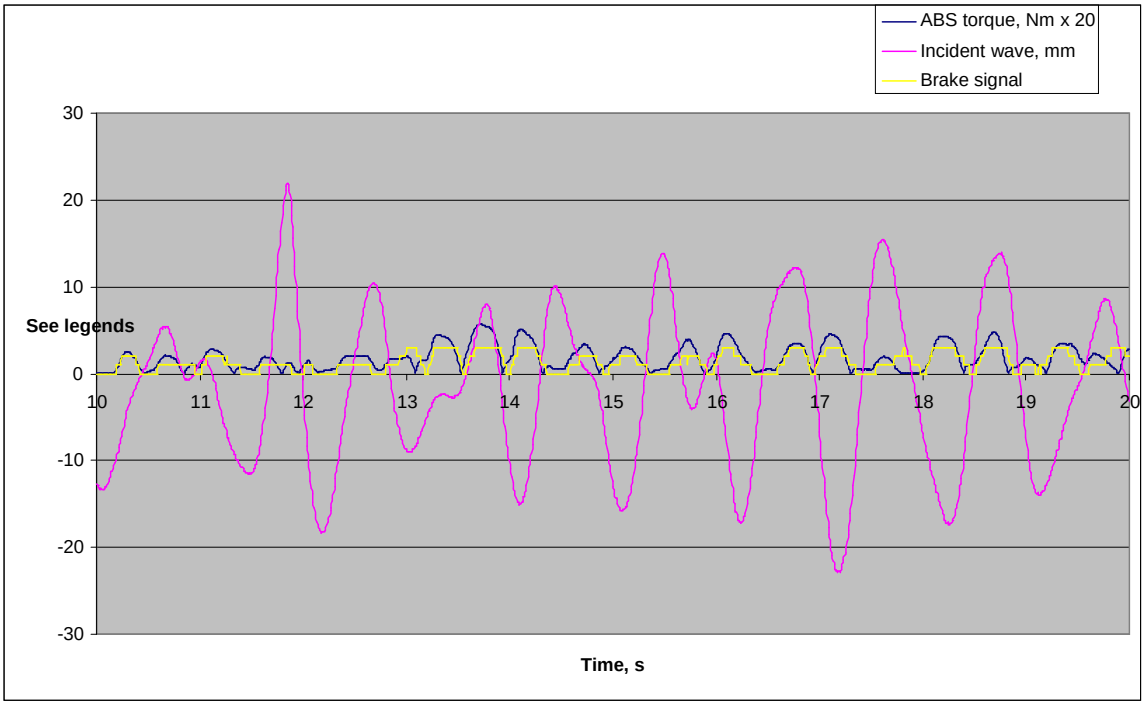

Fig.2.23 Test 87 Incident wave, Brake signal and Torque out

The control system, based as it is on a simple wave probe input, appeared to work quite well but, as was seen, it was far from perfect, If it were there would be a closer correlation between torque and velocity and, probably, greater power.

Nonetheless, the controller was adapting in real time to the wave conditions and testing was continued in a range of wave types to obtain model powers. A typical set of results is shown in Fig.2.25. In this graph the average amplitude-squared results from the row of wave gauges placed ahead of the model are delayed to coincide, approximately, with the power output at the model and both the power levels were obtained by averaging the instantaneous values over a period of 1 second. It can be seen that the two powers vary widely in this short extract and that the absorbed power follows the wave power closely for most of the time.

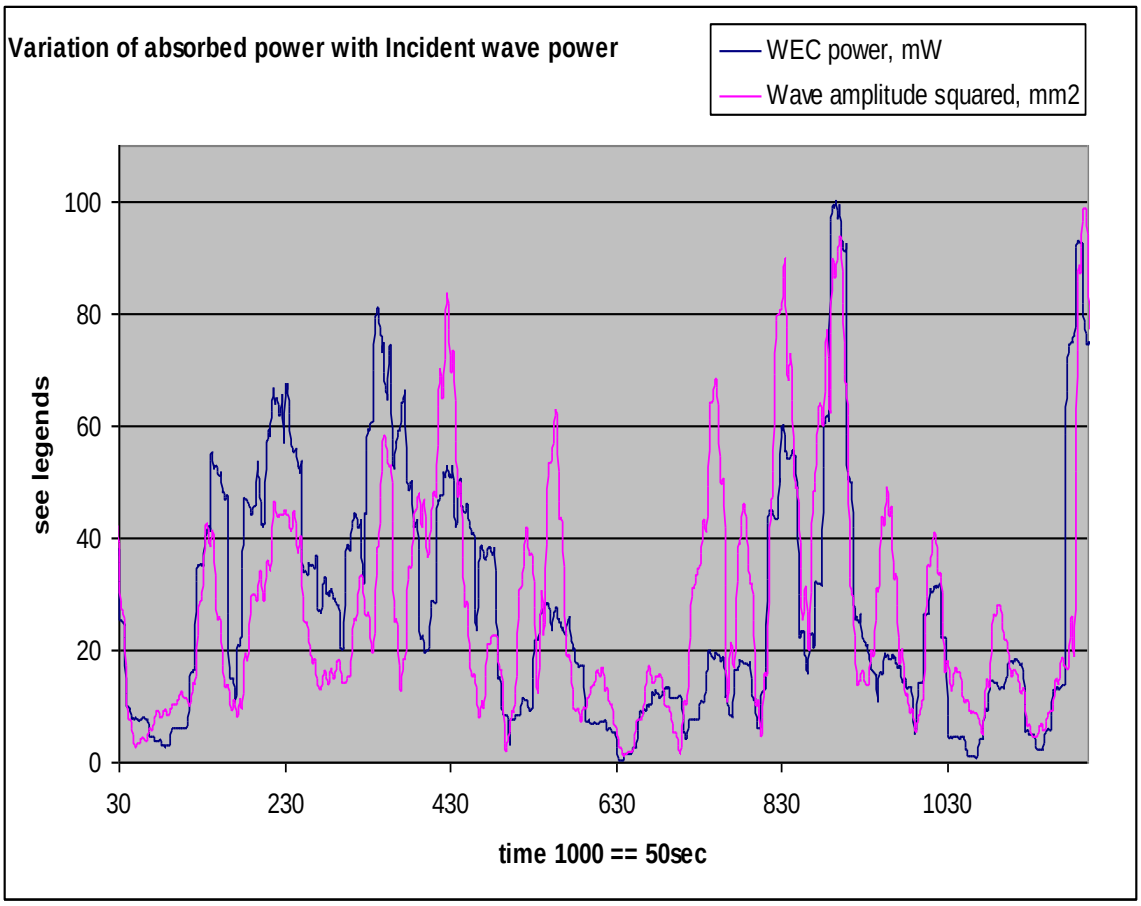

Fig.2.25 Variation in model power and incident wave power from test 150 at EU

2D Mixed waves – power

Fig. 2.26 shows a typical set of results for one wave condition from tests 97-102 at EU. In summarizing such results the peak value of the curve has been taken.

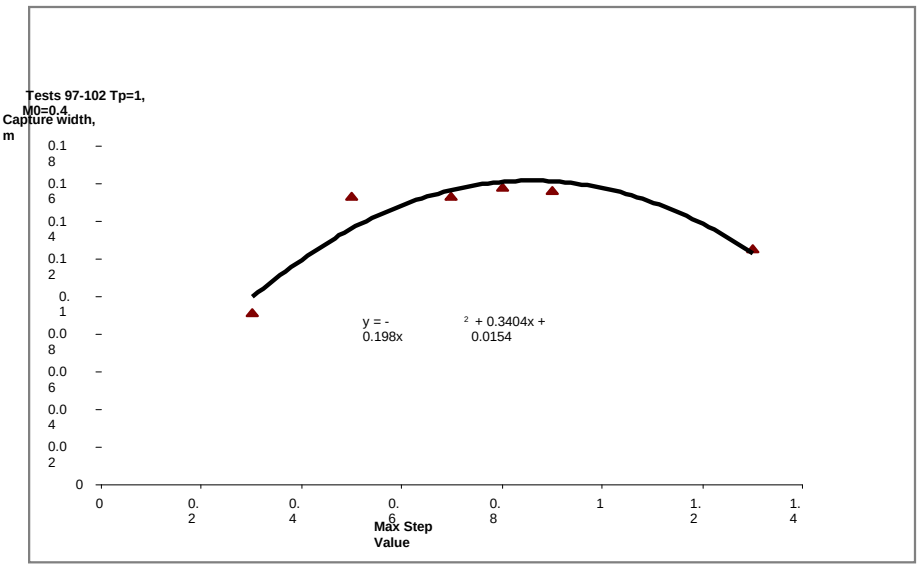

Fig.2.26 Set of results for one wave condition

Fig.2.27 shows the tuned and optimised CW vs. incident wave power. The fitted curve shows the increase in CW with decreasing wave size – as seen in the regular wave results.

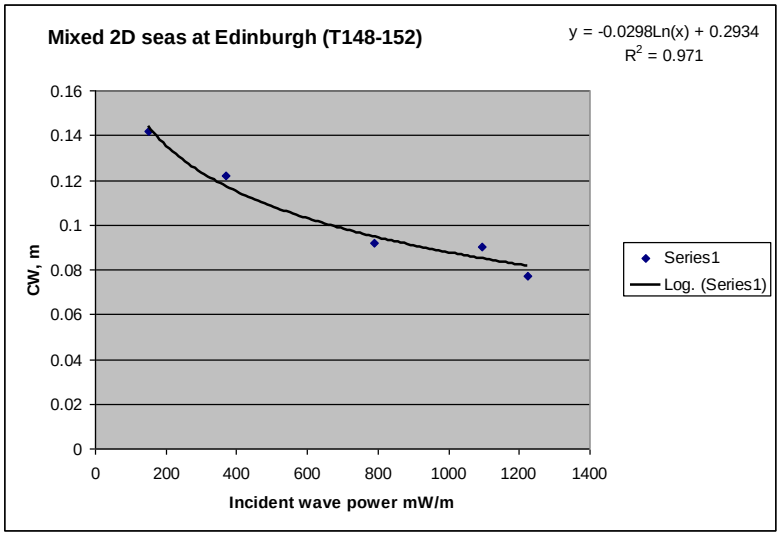

Fig. 2.27 Maximum capture width vs. Incident wave power in 2D mixed seas (fp=1Hz)

3D Mixed-and Spread waves – Effects of degree-of-spread on incident power

Having developed the WRASPA device to the point where its performance in mixed 2D

seas was acceptable we needed to test it in mixed-and-spread seas (3D seas). The Edinburgh University Curved Tank is unique in its ability to create such seas at scales of around 1/100 Atlantic scale and to do this in a repeatable way so that convincing results are obtained. Its design is based on their earlier Wide Tank but by having the wave-makers arranged in an arc ensure that cross-tank "slop" is minimised.

Fig 2.28 examines the effect of spreading function on CW, with Cosn =1 giving the widest spread of directions (centred around the head-on direction) and Cosn=1000 giving almost 2D-like seas. In a fully developed sea state the Cosn value tends to increase as the sea becomes more "focussed". The fitted line shows, for the range of seas used, a small decrease in power when compared with the same seas with "no spread" i.e. long-crested.

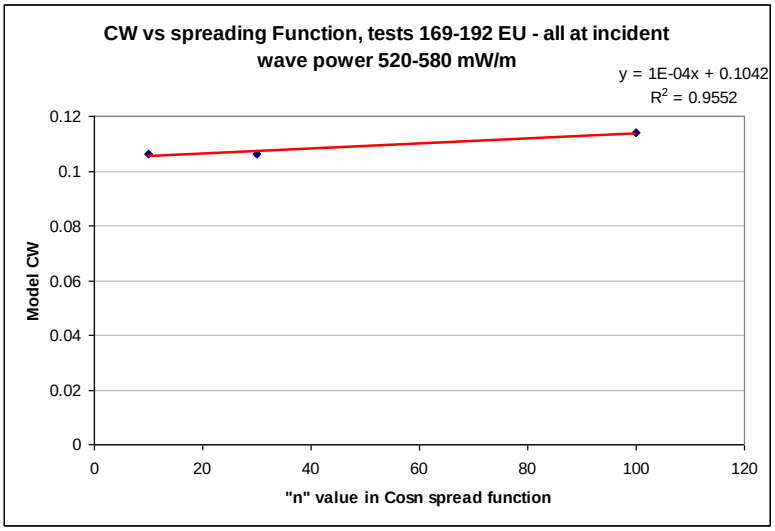

Fig.2.28 Best-tuned power vs degree of spread in mixed-and-spread seas

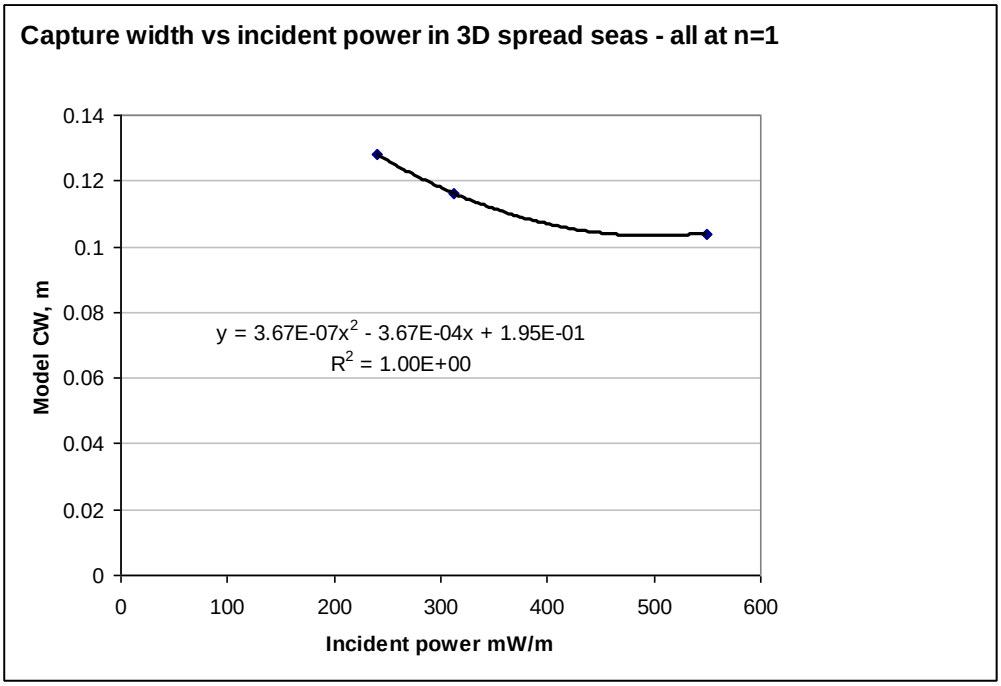

Fig.2.29 CW vs. incident power in un-focussed spread seas.

And Fig.2.29 shows the variation in CW with incident power in spread seas with the value set =1 in the Cosn spreading function. These results would be for the widest spread and the least favourable conditions for power collection. Fig.2.30 compares this result with the equivalents from above for both 2D mixed and regular waves.

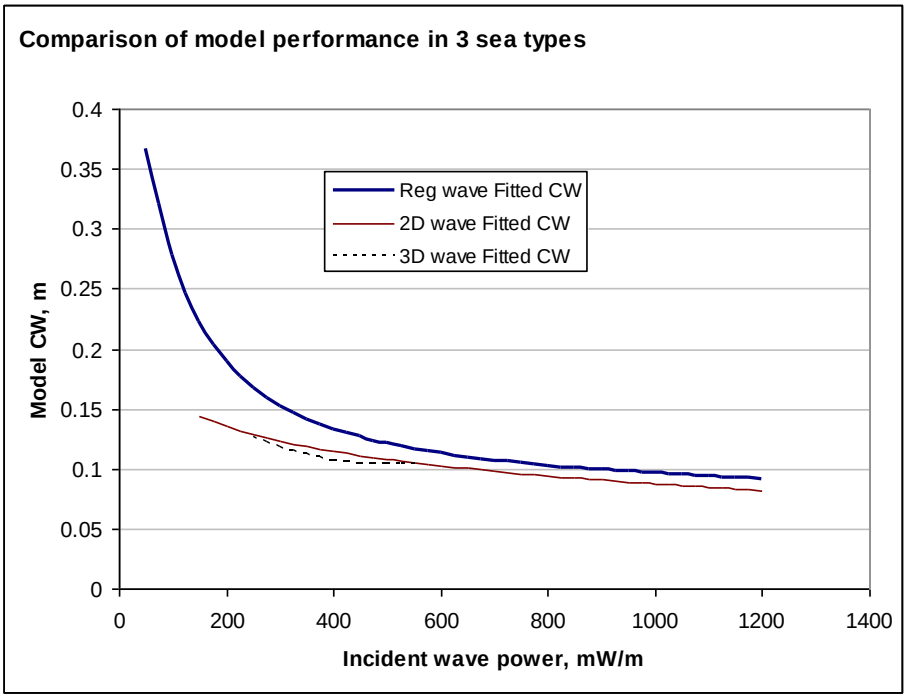

Fig.2.30 Comparing CW's in the 3 sea types

CW in long and short wavelengths (Tests 218-237)

Time did not allow testing over the full rage of wave conditions such as are seen in Fig.2.6 but four conditions were tested at *f*p = 1.4 and 0.83Hz - close to the practical limitations of the tank given the spread of frequencies around these *f*p values. In 2 tests the model remained tuned to 1.05 Hz and in the other 2 it was tuned by raising & lowering the pivot point to make ω_n = 0.89 and 1.25 Hz respectively. In the former case the collector was at its lowest possible frequency, with Fb = 0 and at the other, 1.25Hz. Although ω_n could be made higher it was obvious that further reductions in frontal area would lose power excessively. Fig.2.31 shows the rather unsatisfactory results and suggests that slow tuning may not be as beneficial to this type of WEC as had been thought.

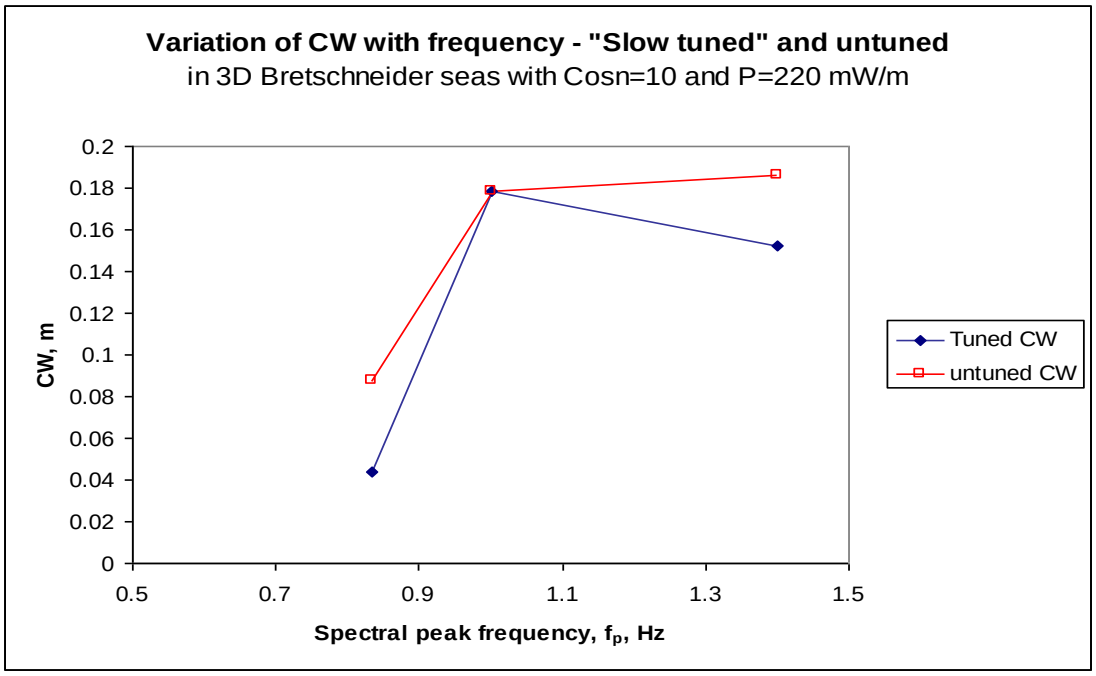

Fig.2.31 Example results at extremes of frequency range

Again, these results appear favourable to the device - indicating that as power decreases, this time with increasing wave frequency, the capture width increases and, vice-versa, decreases with decreasing frequency.

2.2.4 Benchmark testing

In June 2008 in a series of tests in the LU tank the power was measured using the RHM2 collector with fixed levels of damping i.e. without stepwise control. In each test, for a particular combination of pendulum-length and Fb, a decay test in was used to establish its natural frequency, ω_n and the model was then subjected to waves of this frequency and of different amplitudes and at each amplitude the damping level was varied to give torque/velocity graphs. From these optimum CW's were obtained for each condition.

Full Spectrum-Polychromatic Results

A method was then used to convert these regular wave model test results at a range of frequencies and wave amplitudes into annual output in polychromatic seas of equivalent power. From this analysis the annual powers were calculated to be:-

950 kW "raw" power, and
870 kW with power capped at 2MW

These were preliminary results and, as we now have a preferred set of data from the Carbon Trust (Fig.2.6), future tests will use their data for real mixed waves with the collector under control. However, comparing the calculated results with the results shown above from the Edinburgh tests it appears that – comparing them at a central, common wave period, those derived from regular waves overestimate power by a wide

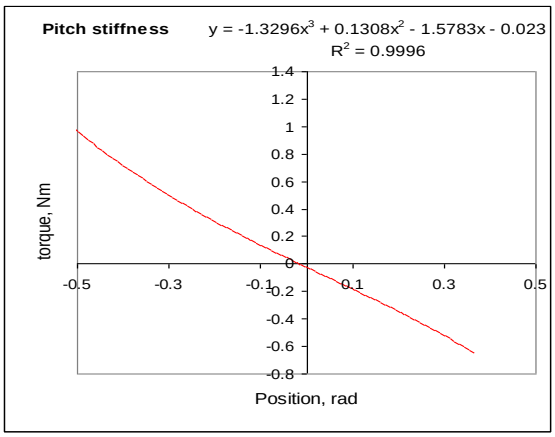

margin. For example at T=10 and Hs = 2.8m derived power CW is given as 20.6m (at full scale) and from tank measurements CW would only be 12m. As the collector would be 25m wide this is equivalent to a capture width ratio of 0.5 approx.

2.2.5 Characterisation tests

These were proposed and adopted as a means of assessing a particular design in relation to another using a relatively simple set of experiments and/or simulations. Also, by conducting a set of 3 parallel tests both in the tank and in flow 3D that we verify the above and build up confidence in the computer model. As is seen in Chapter 2 the correspondence between tank and Flow 3D simulation appears good and with further confirmation, along the lines outlined here, it would be possible to scale up the model in the Flow-3D simulation to full scale and be able to predict full-scale performance with some confidence. The test would be:-

1. Force coeff. (F_1) – the shape is held fixed and waves with freq.= ϖ_n (its resonant freq.) and of differing amplitudes act on it. A graph relates torque to amplitude (see Fig.2.33)

2. Free motion – Collector is free to move in pitch and similar waves to the above act on it. Another graph relates angular motion to amplitude. (see Fig.2.34)

3. Decay test – the collector is free to move in still water and is released from a position θ_0 of say +0.2 rad and the decay curve is recorded. (see Fig.2.35)

From these and with a knowledge of the pitch stiffness of the collector (e.g. see Fig.2.32) we can obtain constants for the 1 DOF equations below, including viscous drag. Changes in this term with scale are difficult to predict, but using the Flow 3D model, calibrated in this way it would be possible to account for all the expected effects and to re-run the model at full scale with confidence.

Fig. 2.32 Pitch stiffness in still water - from test 217

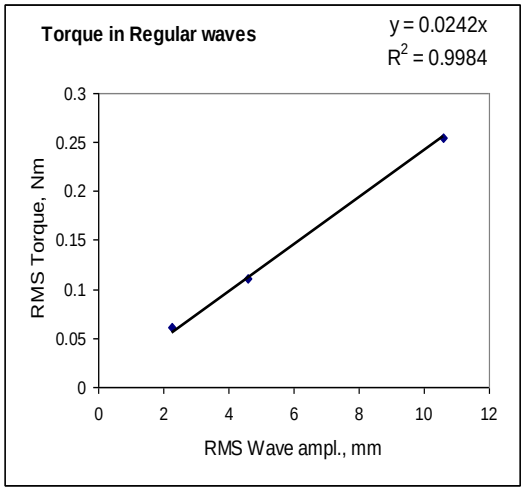

Fig. 2.33 Torques acting on a fixed collector

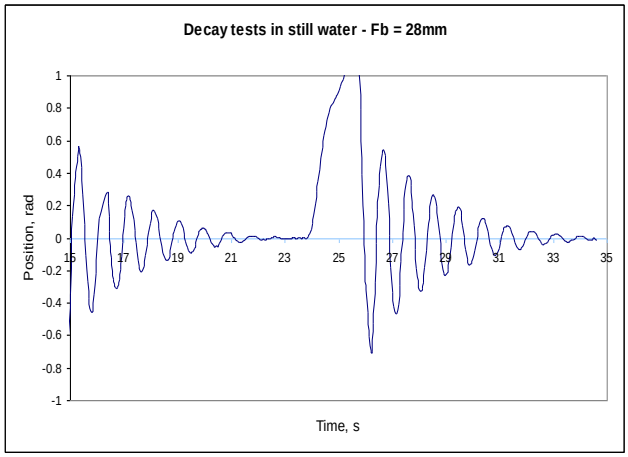

Fig. 2.35 Decay tests in still water

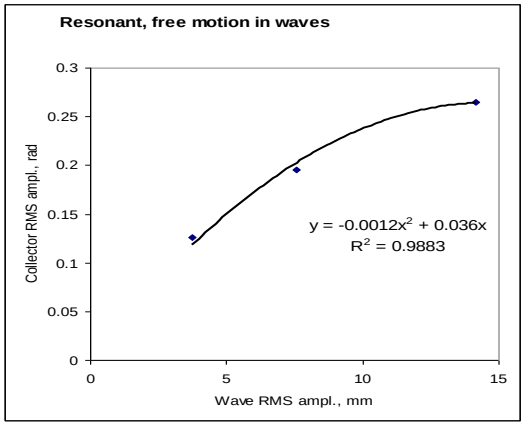

Fig. 2.34 Free motion of collector in waves

2.3 Discussion

2.3.1 Mathematical models

Discounting higher-order effects, the dynamics of the WRASPA device can be modelled as a rotational spring-damper system using a second-order differential equation in terms of the angle of pitch, θ, thus:-

$$(I_Q + a_{55})\ddot{\theta} + b_{55}\dot{\theta} + c_{55}\theta = (q - p)F_1\alpha \quad \text{.....(1)}$$

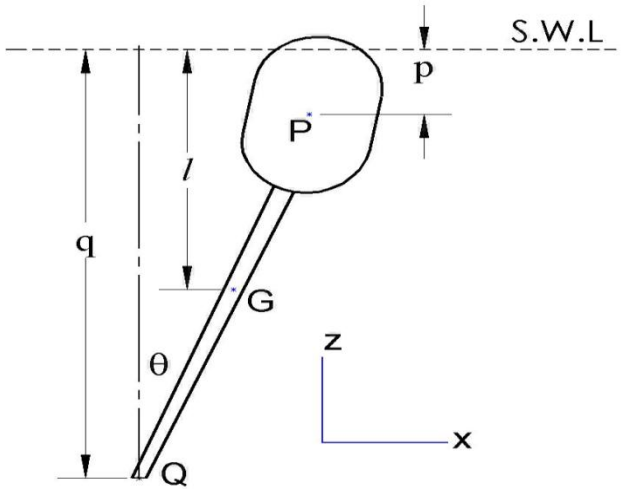

Figure 2.36: schematic diagram

The frequency-dependent hydrodynamic parameters (a55, b55 and F1) and the hydrostatic parameter, c55, are derived using the commercial code WAMIT™ at intervals of 0.5 radians per second up to 10 radians per second. In the program a three-dimensional panel method using potential theory is implemented. WAMIT solves the equation of motion in the frequency domain. The body surface is discretized so that a 'critical frequency' can be determined. The critical frequency is specified to satisfy the validity criteria of a minimum wavelength greater than seven times the maximum panel dimension. The critical Frequency in this case, is 21.19 radians per second (3.37Hz), well in excess of the highest required frequency.

In WRASPA, if we add terms for the PTO torque and for viscous drag, equation 1 can be re-written as:-

$$F_1\alpha(p - q) = \ddot{\theta}(a_{55} + I_Q) + \dot{\theta}(b_{55} + \Lambda) + \theta.c_{55} + \dot{\theta}\,|\,\dot{\theta}\,|\,d_{55} \quad \text{.....(2)}$$

With PTO switched off this reduces to:-

$$F_1\alpha(p-q) = \ddot{\theta}(a_{55} + I_Q) + \theta.b_{55} + \theta.c_{55} + \theta|\theta|d_{55} \quad \ldots\ldots\ldots\ldots\ldots\ldots(3)$$

and in still water, with no wave force, it becomes:-

$$0 = \ddot{\theta}(a_{55} + I_Q) + \theta(b_{55} + \Lambda) + \theta.c_{55} + \theta|\theta|d_{55} \quad \ldots\ldots\ldots\ldots\ldots\ldots\ldots(4)$$

The drag coefficient d_{55} was thought by the author to be a significant factor but the following analysis, based on experiments refutes the idea:-

Using equation 4 and results from tests 210-216, values for factors F_1, a_{55}, b_{55} and c_{55} were obtained and by inserting them into a torque equation in an "Excel" time-step simulation, a decay curve similar to Fig 2.35 was obtained and by small alterations to the coefficients an exact replication of the decay curve was found with:-

$a_{55} = 0.0035$ kgm^2, $b_5 = 0.529$ Nsm, $c_{55} = 1.58$ Nmrad^{-1} and $d_{55}=0$

These values correspond well with ones from WAMIT analyses [2.6] for a similar shaped collector at the same freeboard and frequency.

2.3.2 Alternative forms and concepts

In the project proposal it was suggested that other collector mechanisms be considered. These are described below:-

Four-bar concept

In this the collector body would be linked to the base unit by a 4-bar linkage whose motions would be damped by a hydraulic PT0 system. Its main advantage was in increasing the Spring stiffness and thus, natural frequency for a collector of given volume. Its vulnerability to extreme wave forces and lack of tune-ability led to it being ruled out in preference to the "Hammerhead" concept - see below in Appendix C or, possibly, a 2-bar version in which the collector could "feather" in extreme conditions and so have better survival properties.

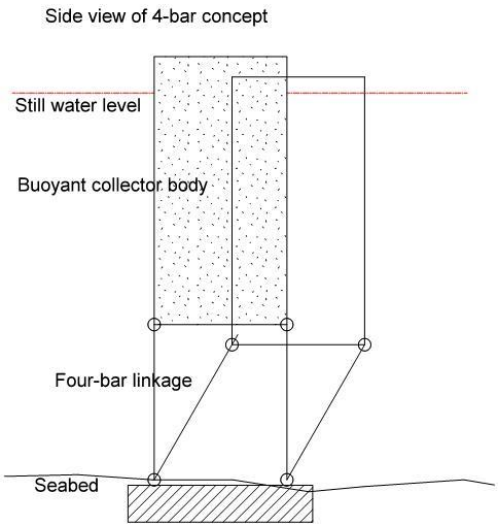

Fig.2.37 diagram of 4-bar concept

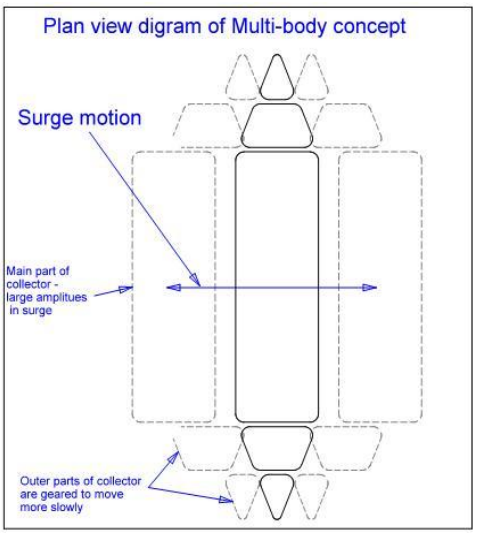

Multi-body Types.

Fig.2.38 – plan view diagram of multi-body type

In this concept it was proposed that, as viscous drag at the edges of the collector appeared to be a primary cause of power loss, these edges should be caused to move more slowly than the main, central part, of the collector. (See Fig.2.38) This might be effected by hydraulic gearing. In discussions it was agreed that this mechanism would be too complex as an add-on to WRASPA as it existed so consequently this line was not pursued further.

Hammerhead concept

This is described in a draft patent in Appendix C as a means of "increasing the rotational stiffness of the collector using buoyant bodies ahead and astern of the collector". These bodies would occupy some of the volume normally occupied by the added mass of water and would have the effect of reducing cost by reducing the collector volume and, thus, the amount of ballast needed. There was not enough time to test the idea but it remains an interesting possibility. If desired the buoyant bodies might be moved towards and away for the central plane of the collector e.g. by hydraulics and so be used in "slow" tuning.

Seabed Fixing.

Initial proposals for WRASPA included a large diameter mono pile drilled or driven into the seabed. It is accepted that this one aspect might so dominate costings as to make the whole device uneconomic. As an alternative it is proposed that the base unit should be housed in a pre-fabricated "spider" unit that might look as Fig.2.39 the large bending moment being resisted by strong points holding down the feet. These strong points might comprise a central high-strength stainless pin grouted into a hole of sufficient depth to give holding forces of several hundred tonnes, depending on arm length and extreme load predictions.

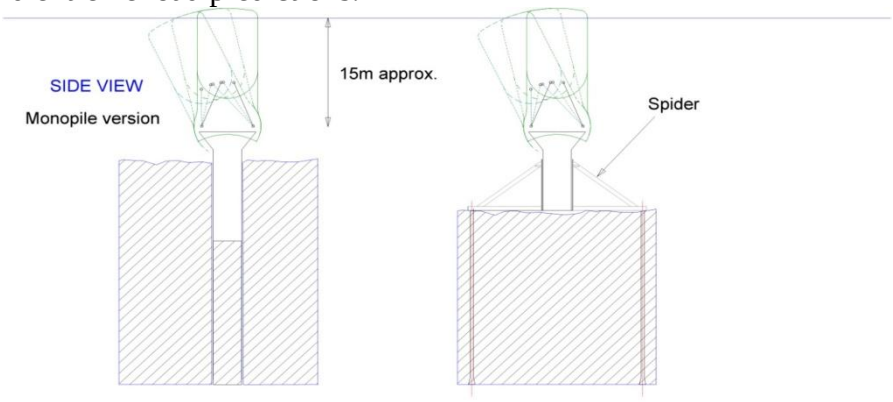

Fig.2.39 Seabed mounting alternatives

2.4 Achievements/ Outputs (Papers etc.)

2.4.1 Aggidis, G.A., Rahmati M.T., Chaplin RV, McCabe AP, Mingham CG, Causon DM, Bhinder MA "A control system for a new wave energy converter in irregular wave climates," 28th ASME International Conference on Ocean, Offshore and Arctic Engineering, Honolulu, Hawaii, 31 May-5June 2009.

2.4.2 Bhinder MA, Rahmati M.T., Aggidis, G.A., Chaplin RV, Mingham CG, Causon DM "Numerical & Experimental Flow Analysis of a Wave Energy Converter, Proceedings of The 8th European Wave and Tidal Energy Conference, Uppsala, Sweden, 7-10 September 2009.

2.4.3 Bhinder MA, Rahmati M.T., Aggidis, G.A., Chaplin RV, Mingham CG, Causon DM "Numerical and Experimental Study of a Point Absorbing Wave Energy Converter in Regular and Irregular Waves," International Conference on CLEAN ELECTRICAL POWER, Renewable Energy Resources Impact, Capri, Italy, June 9th-11th, 2009.

2.4.4 Chaplin RV, Rahmati M.T., Gunura, K and Aggidis, G.A., "Control systems for WRASPA," International Conference on CLEAN ELECTRICAL POWER, Renewable Energy Resources Impact, Capri, Italy, June 9th-11th, 2009.

2.4.5 Bhinder MA, Rahmati M.T., Aggidis, G.A., Chaplin RV, Mingham CG, Causon DM, "A Joint Numerical and Experimental Study of a Surging Point Absorbing Wave Energy Converter," 28th ASME International Conference on Ocean, Offshore and Arctic Engineering, Honolulu, Hawaii, 31 May-5June 2009.

2.4.6 Rahmati M., Aggidis G.A., Chaplin R.V., and McCabe A.P., Investigating a Power-Absorber Wave Energy Converter, Proceedings of POWER 2008, ASME International Power 2008 Conference, Orlando, Florida, USA, July 22 to 24, 2008.

2.4.7 Rahmati M., Aggidis G.A., Chaplin R.V., and McCabe A.P., Test on a Novel Pitching-Surge Wave Energy Converter, Proceedings of World Renewable Energy Conference WREC 2008, Glasgow, 19-25 July 2008.

2.4.8 Chaplin R.V. and Aggidis G.A., WRASPA: Wave Interactions and Control for Pitching-Surge Point-Absorber Wave Energy Converters, Proceedings of the 7th European Wave and Tidal Energy Conference, Porto, Portugal, 11-14 September 2007.

2.4.9 Rahmati, M.T., McCabe, A.P., Aggidis, G.A., Chaplin R.V., Investigating a power absorber wave energy converter, ASME Power Conference 2008, Date: JUL 22-24, 2008 Lake Buena Vista FL, PROCEEDINGS OF THE ASME POWER CONFERENCE 2008 Pages: 699-705, Published: 2008.

2.4.10 Chaplin R.V. and Aggidis G.A., An Investigation into Power from Pitch-Surge Point-Absorber Wave Energy Converters, published by IEEE, Clean Electrical Power, 2007. ICCEP '07, ISBN: 1-4244-0632-3, INSPEC Accession Number: 9739979, Digital Object Identifier: 10.1109/ICCEP.2007.384264, Posted online: 2007-07-16 13:19:33.0, pp 520-525 Publication Date: 23 May 2007.

2.5 Future Work

- Improve collector shape and reduce its volume. WRASPA could be smaller and more economic. Drag must be reduced, possibly by eliminating sharp changes in velocity underwater and their attendant losses.

- Examine the slow-tuning requirements over the full spectrum – see Edinburgh results

Control

- An in-depth study of the stepwise control method should be conducted to maximise potential power capture in mixed seas. However, the choice of wave elevation as the input parameter seems mistaken and others should be investigated e.g.the collector velocity, as proposed by Salter et al [1.5] This should be done in parallel with a technical-economic study in comparison with the commercially available Artemis or equivalent.

Deep Water Versions

- Once a WRASPA-type WEC is perfected its economics would be improved by adopting Prof French's [1.4] Superwec idea.

Inter-Device Comparisons

- In line with the Carbon Trust's dictum that any proposed development of device or subsystem shall be objectively compared with existing, leading technologies. These might be taken as:-

- For deep water, the Salter / Edinburgh Duck as an elegant, logical and, arguably, well proven device. The Pelamis device is currently providing a proving method for the central spine and the Artemis PT0 is finding acceptance in parallel fields. So, although the Duck has not yet been deployed at full-scale it is conceivable that it could be, and within a predictable time frame.

- For shallow water, near-shore, the Oyster with its water hydraulics and on-shore power conversion system appears as if it will be a front-runner.

- Both these devices have powerful methods for dealing with the huge torques found in wave power - the Duck by phase diversity between Ducks and the torsional strength of the spine and Oyster by allowing +/- 90 degrees excursion in the collector, at controlled torques, and by taking advantage of the mainly horizontal motion of the body of water and using this to minimise costly collector torque and maximise motion.

2.6 References (section 2)

2.1 Chaplin, R V, "Surging Point-absorber behaviour" – Internal laboratory note. Lancaster 2006

2.2 Evans D V "Some analytic results for 2D and 3D wave energy absorbers" pp. 213-249 in "Power from Sea Waves" Ed. Count, B M, Ac. Press 1980

2.3 Chaplin, R V and Aggidis, G A "Wave interactions and control in a new pitching-surge point-absorber wave energy converter" Proc. 7th EWTEC Conf., Porto, Portugal, 2007

2.4 French, M J "On the difficulty of inventing an economical sea wave energy converter: a pers9onal view" Proc. I Mech E Vol.220 Part M, 2006

2.5 Salter, S et al. " Power conversion mechanisms for wave energy" Proc. I Mech E Vol 216 Part M, 2002

2.6 McCabe, A, "W1 Hydrodata" internal lab report giving WAMIT analysis results for WRASPA collector RHM1, 2008.

3. Numerical Modelling

3.1 Introduction / Methodology

The motion of WRASPA in response to incident waves was numerically modelled successfully at Manchester Metropolitan University (MMU). A commercial CFD (Computational Fluid Dynamics) code was used due to the short time duration of the project. Choosing a suitable CFD package was not an easy task due to the lack of available case studies related to this specific problem. Knowledge gained in this project may be valuable for future research into similar problems.

Numerical study of WRASPA requires accurate modelling of water waves and such cases involve a free-surface. Various incident waves were modelled and WRASPA's response to these incident waves was monitored and then compared with corresponding experimental data.

The following main stream CFD packages were considered for initial tests.

- STARCCM+
- ANSYS CFX
- FLOW-3D

A preliminary analysis of all these packages was conducted and the abilities of these packages to model water waves and wave-structure interaction were compared in terms of accuracy and robustness. Further detail of the findings from all these three codes is given in next sub-sections.

3.1.1 STARCCM+

In the preliminary tests it was observed that although water waves can be modelled in STARCCM+, the code (v3.02) was unable to compute the surging motion of the device due to the limited mesh deformation ability. However later versions (v3.04 and v3.06) have claimed this ability but they were not available at the time.

3.1.2 ANSYS CFX

CFX was found to be able to model the wave climate and also to simulate the surging motion of the device by using its unstructured deforming mesh capability. A number of simulations were run to investigate wave propagation and the times to set up and compute the problem were recorded. A 3D view of the mesh structure used within the numerical wave tank (NWT) of CFX is shown in Figure 3.1 and the propagation of a linear wave at two time instants is shown in Figure 3.2.

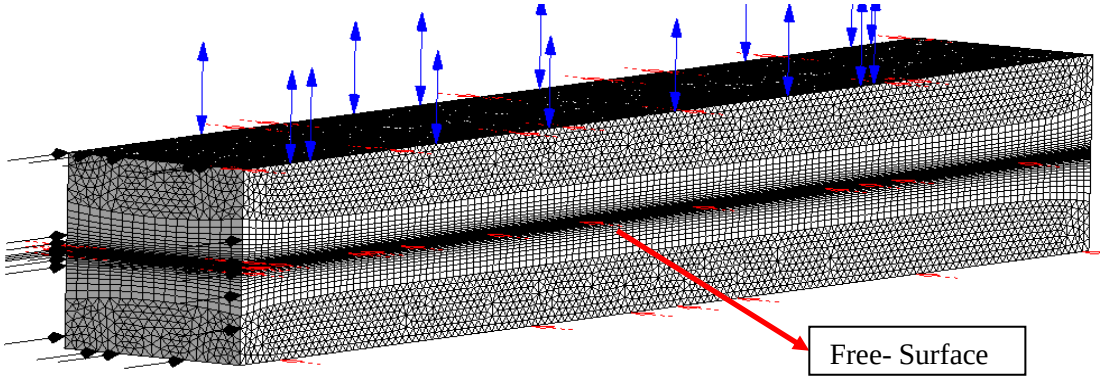

Figure 3.1: Mesh structure of a 3D numerical wave tank in CFX.

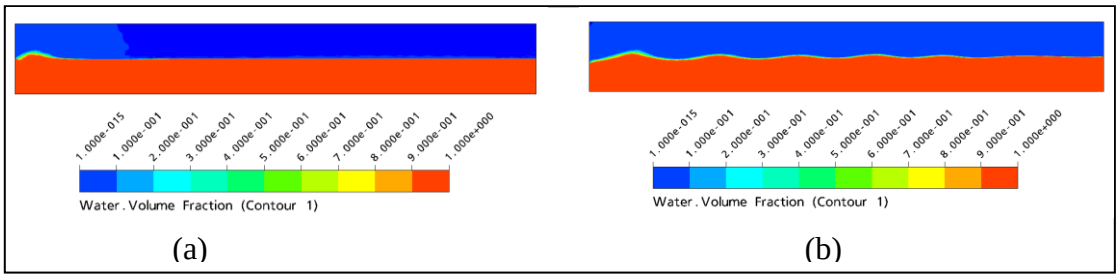

Figure 3.2: Linear wave propagation in the numerical wave tank of CFX at time T seconds. (a) T = 1.0, (b) T = 9.25.

3.1.2.1 Issues encountered in CFX

- The wave dissipation rate was found to be quite high. Due to this reason it was difficult to obtain the exact incident wave at the device.

- Reflection of waves from the outflow (right hand) boundary of the numerical wave tank was one of the major issues. In the numerical wave tank the reflected waves interfere with the incoming waves causing an undesired wave climate around the device.

- The solver was slow. It took 2 days to simulate 15 seconds of linear 3D waves (without having any device in the tank) using 436122 cells on the following machine: Intel(R) Core(TM)2 Duo CPU E6750@2.66GHz , 8GB of RAM. This shows that a 15s simulation of the device in operating mode would require more than 5 days to complete.

- The time required for setting up the simulation was estimated and compared among all codes. This included geometry creation, meshing and then specifying the boundary conditions for the computational domain. In CFX the free-surface requires a fine mesh which was achieved by slicing the whole domain at the free-surface and then prescribing an inflation layer in the inner plane (Figure 3.1). However as WRASPA sticks out from the free-surface (Figure 3.3) the strategy failed. Consequently, to fulfil all the requirements of a deforming mesh became prohibitively time consuming with CFX.

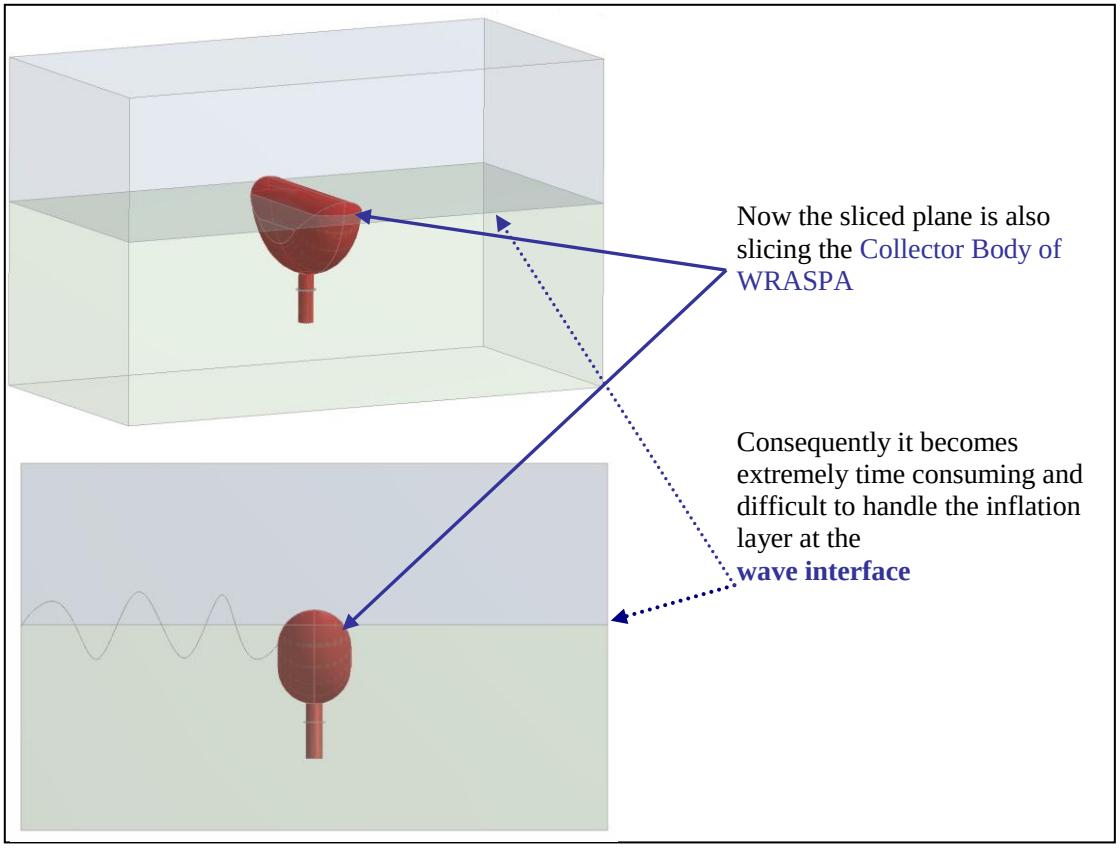

Figure 3.3: Mesh issues within CFX.

3.3.3 Flow-3D

Flow-3D's one fluid model (single fluid with free-surface) was used to test wave propagation. It was observed that the decay in the wave's amplitude (as it propagates) is much less than observed in CFX and the solver was found to be relatively efficient in terms of computing time. A 3D simulation of a wave in a tank of dimensions 35m x 2.5m x 1.5m took about 5 hours using 793638 cells. Flow-3D uses a structured mesh for its computational domain. Use of a single fluid with a free surface is based on the idea of volume fraction (F). Thus F=1 in the fluid region and F=0 in the other part of the domain (named the void region). 'Void regions' have uniform pressure assigned and there is no fluid mass in these regions. Unlike CFX, this model does not require extra cells at the free surface hence reducing both setup and simulations run time. The ability to modify the mesh and geometry shape independently was another help in reducing simulation setup time.

The surging motion of the WRASPA device was modelled using the General Moving Object (GMO) model of Flow-3D. The GMO model offers a fixed mesh method to simulate moving objects within the computational domain. The model was found to be robust and accurate. Instead of a deforming mesh, the option of using a fixed mesh method was found to be quite efficient in terms of computing time.

Considering above mentioned advantages, it was decided to use Flow-3D for the numerical modelling of the WRASPA device. For all simulations, the shared memory parallel (SMP) version of Flow-3D (v 9.3.1) was used. This version uses all available processors on the same machine which can also be regarded as locally parallel.

3.1.3.1 Simulation Setup in Flow-3D

Simulation setup in Flow-3D is explained step by step in this section. The geometry file was imported into Flow-3D in .STL format (from SolidWorks). Further detail about setting up the simulation is given below.

In Flow-3D rigid structures were defined by using a technique named FAVOR™ . This technique is based on the concept of area fraction (AF) and volume fraction (VF) in a rectangular structured mesh. As the shape of the rigid body depends on the areas and volume fractions of occupied cells, a locally fine mesh was needed to get the exact geometric shape of the rigid body. The rendered output of the collector shape using two different (coarse and fine) meshes is illustrated in Figure 3.4. An optimum mesh was obtained by using nested mesh blocks (Figure 3.4, 3.5). The option of adding nested blocks allowed fairly easy insertion of extra cells in the region around the collector.

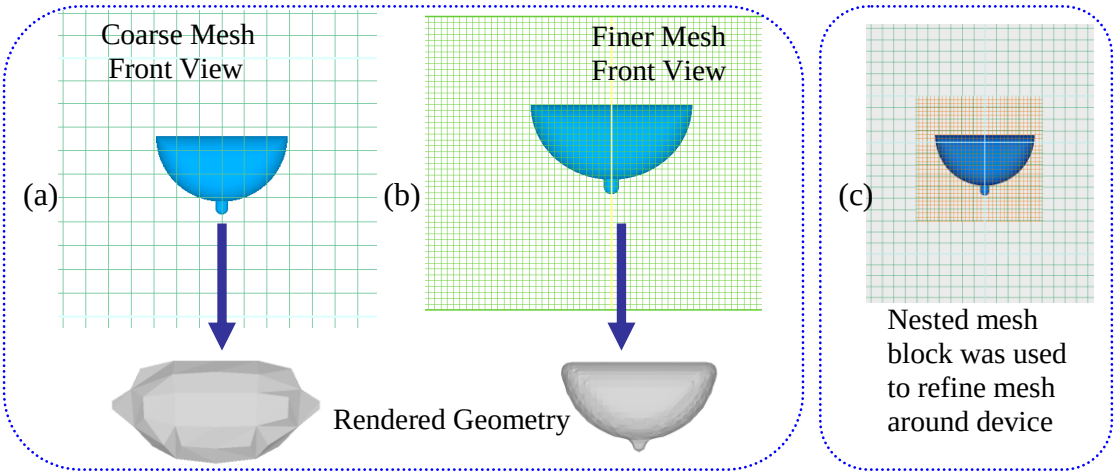

Figure 3.4: Rendered geometry against defined mesh (a) coarse mesh (b) Fine mesh (c) combination of (a) and (b) using nested block option.

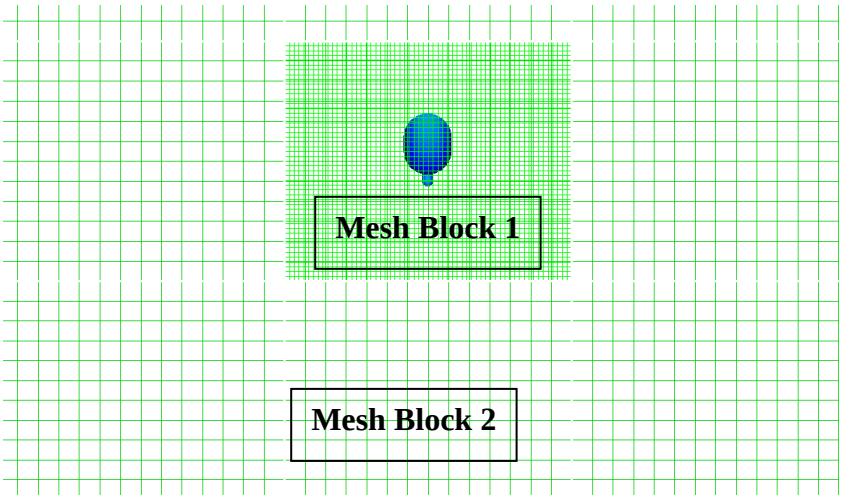

Figure 3.5: Side view of the computational domain showing nested mesh blocks .

Boundary conditions applied to the numerical wave tank are explained by labels in Figure 3.6 and Table 3.1. To minimize wave reflection from the downstream (right hand) end of the wave tank the outflow boundary condition was applied together with stretched cells adjacent to this boundary to numerically dissipate any reflected waves (Figure 3.7).

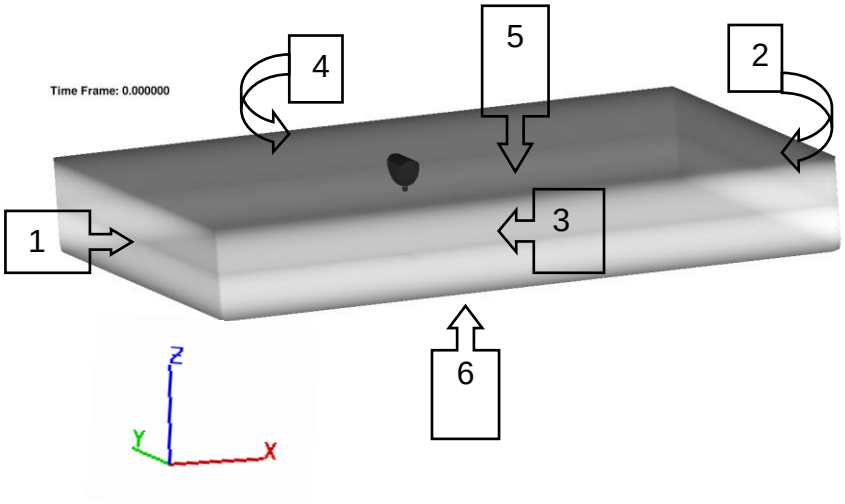

Figure 3.6: Face labels refer to the boundary conditions explained in Table 3.1.

Table 3.1: Boundary Conditions Explained

Face Number	Face of NWT	Boundary condition
1	Left - Low X	Wave Inlet
2	Right - High X	Outflow
3	Front - Low Y	Symmetry
4	Back - High Y	Symmetry
5	Top - High Z	Fixed Pressure
6	Bottom – Low Z	Wall

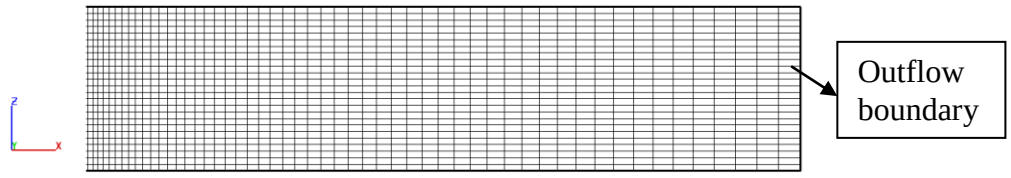

Figure 3.7: Segment of NWT showing stretched cells used adjacent to the outflow boundary to reduce wave reflections.

At the free-surface a constant pressure of 1atm was specified by prescribing this pressure in the void region. This was done by defining the top boundary as a fixed pressure boundary of value 1atm. The initial hydrostatic pressure profile within the

fluid is given in Figure 3.8. Also as part of the initial conditions the still water level was specified by defining the fluid height at each boundary. This gives the correct water depth inside the wave tank and ensures that the required free-board is set correctly.

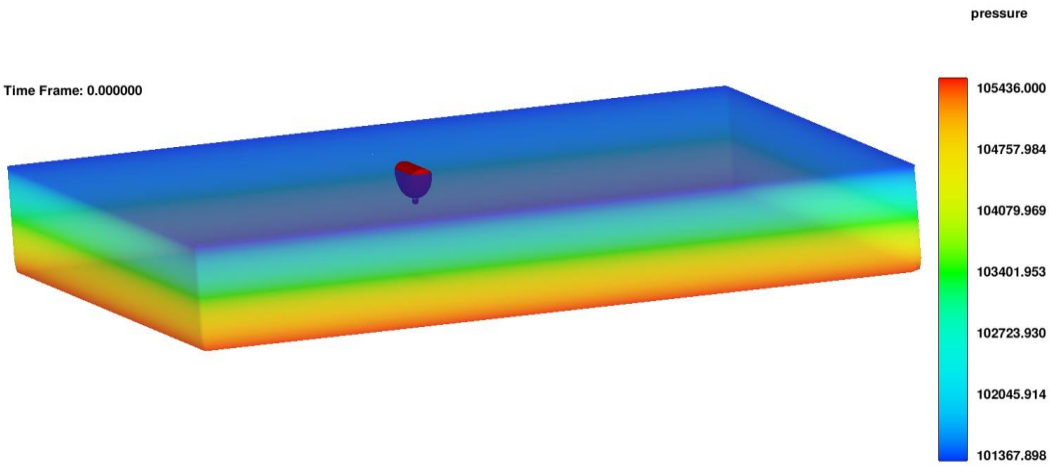

Figure 3.8: Initial hydrostatic pressure profile in numerical wave tank.

Table 3.2 lists the model properties used in the simulations.

Table 3.2: Model Properties

Flow mode:	Incompressible
Number of fluid:	One fluid
Moving Object Model:	Implicit
Turbulent Model**:**	Renormalized group (RNG) model
Pressure Solver:	Implicit, GMRES
Volume of Fluid Advection:	Split Lagrangian Method
Momentum advection:	Second order monotonicity preserving

3. 2 Results

The device was tested numerically and the results were compared with small scale tank tests conducted at Lancaster University. To ensure that the results obtained were mesh independent, tests with three different mesh sizes around the device were conducted as explained below.

3.2.1 Mesh Independence Tests

In these tests three different mesh sizes (for block 1) were used for the same simulation and the results of each test were compared (Figure 3.9) along with CPU time. In each test the mesh size of block 2 was kept constant. Table 3.3 shows the total number of cells, the smallest cell size (in the whole tank) and the time taken for each case. It can be seen (Figure 3.9) that the 3 meshes gave practically the same results. Therefore mesh 1 was used for subsequent simulations to speed up compute time.

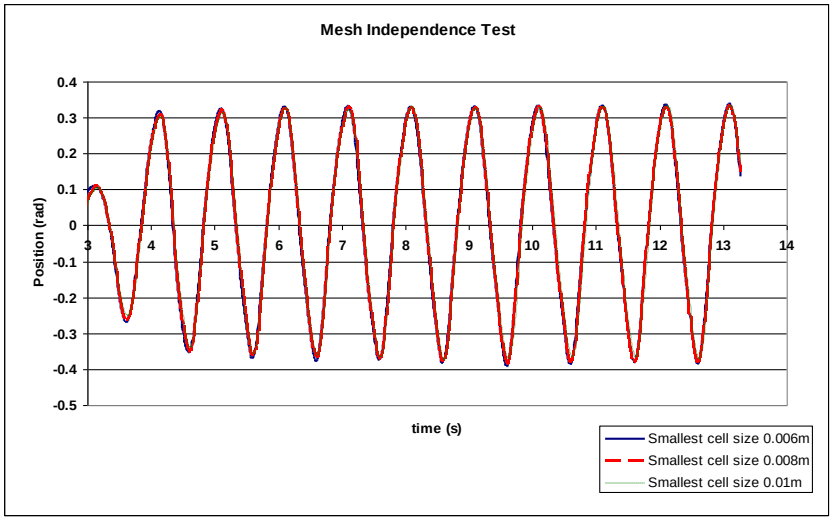

Figure 3.9: Results showing mesh independence of the solution.

Table 3.3: Details of Each Simulation Run For Mesh Independence Test.

Mesh	Total number of cells	Smallest cell size (m)	Time taken by solver for a 13 sec run
1	991188	0.01	1day 8hr
2	1252904	0.008	1day 14hr
3	1968372	0.006	3days

The numerical tests can be divided into the following categories and explained.

3.2.2 Decay Test

This test was used to measure the natural frequency of the device. For this purpose the device, from its resting vertical location in still water, was pulled towards one end and held for a few seconds so that the disturbed free surface became calm. Then the device was released and its damped oscillatory motion was measured. Numerical modelling of this test was conducted in two separate stages (Figures 3.10, 3.11). Firstly, the device was moved to 0.4rad from the vertical by assigning a constant velocity on the walls of the collector body for 3 seconds and was held at 0.4rad for another 1 second to allow time for the water surface to return to its initial calm state. Secondly, starting from the result file of the first stage, the device was released.

From the experimental results it was found that the natural frequency of the device was a function of free-board and pivot depth. This natural frequency should equal the incoming wave's frequency to get maximum power output. From the decay test the optimum value of the free board and pivot depth was found (to tune the natural frequency of the device to 1Hz approx). A comparison of numerical and experimental results for the decay test is given in Figure 3.12.

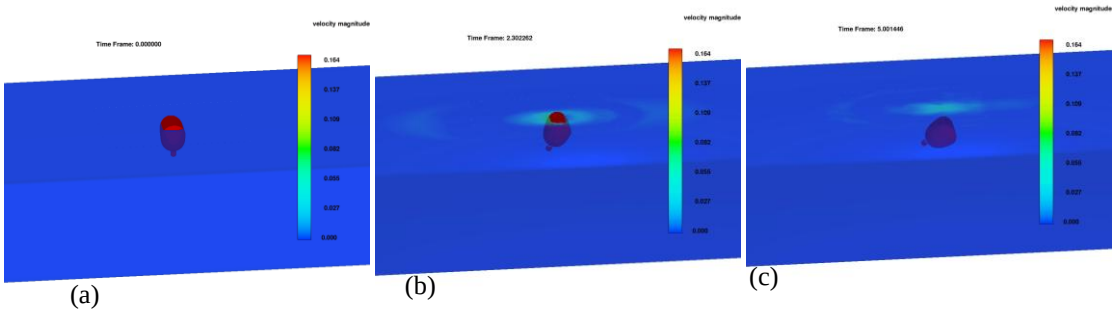

Figure 3.10: First stage of the decay test: (a) initial position, (b) medium deflection (c) maximum deflection

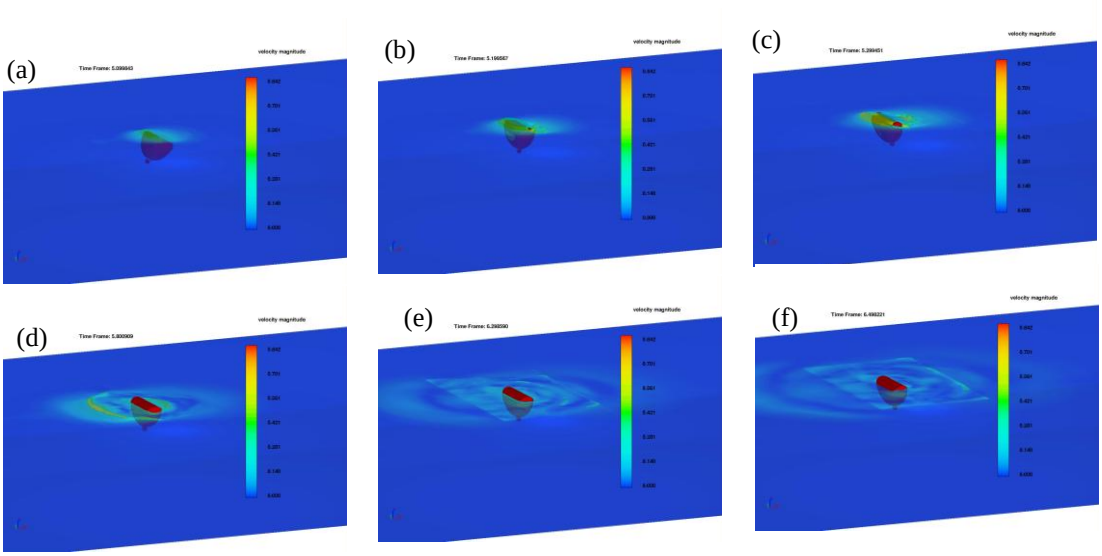

Figure 3.11: Second stage of the decay test at t seconds (a) t=0 (b) t=5.20 (c) t=5.30 (d) 5.80 (e) t=6.30 (f) t=6.50

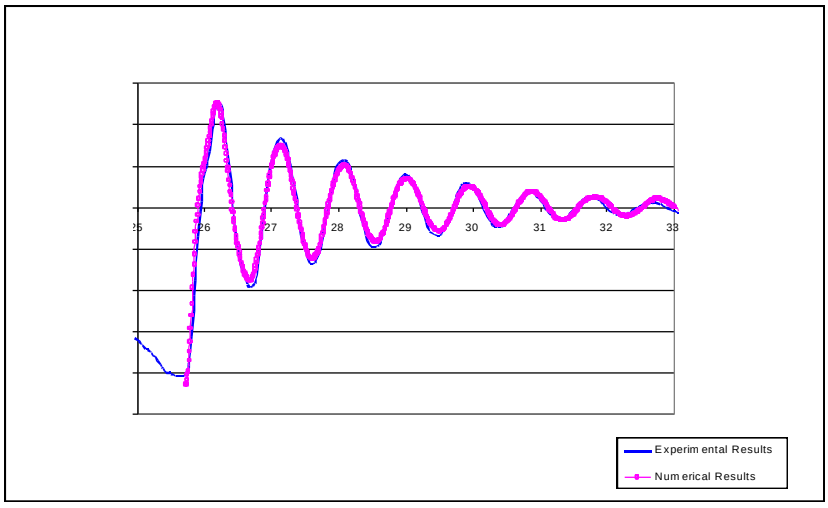

Figure 3.12: Comparison of experimental and numerical angular displacements over time in the decay test.

3.2.3 Free Pitch Motion Test

In this test the (free) motion (i.e. control system turned off) of the WRASPA device in response to incoming waves was simulated. This test was conducted for two different wave amplitudes. A schematic of a WRASPA design (RHM2) is depicted in Figure

3.13 showing a typical simulation configuration used in the NWT. The angular displacement of the device against time was plotted and compared with experimental data (Figures 3.14, 3.15).

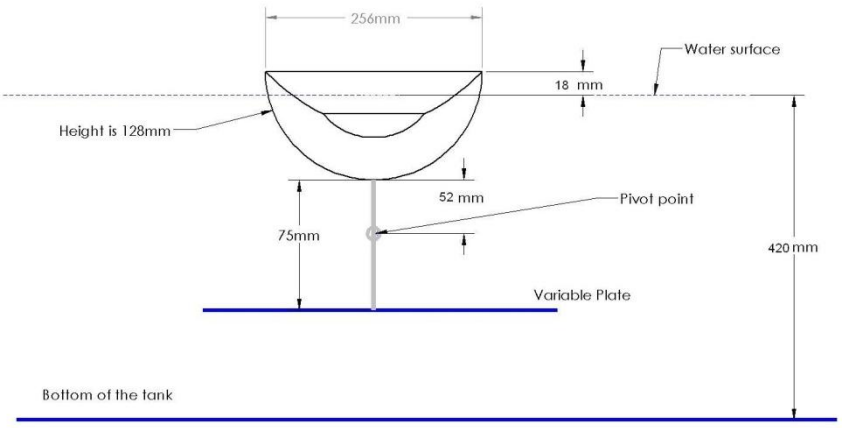

Figure 3.13: Schematic showing a front view of WRASPA (RHM2) in the Numerical Wave Tank.

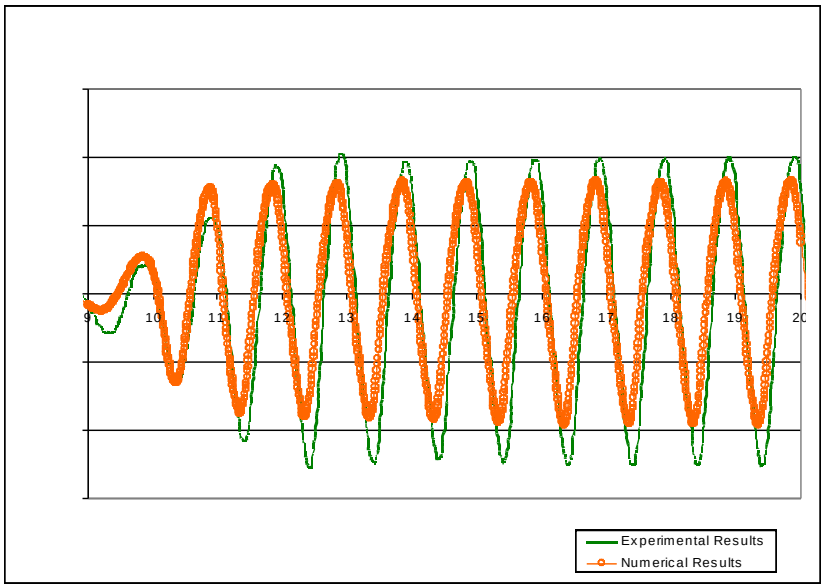

Figure 3.14: Angular displacement of WRASPA against linear waves of 10mm amplitude.

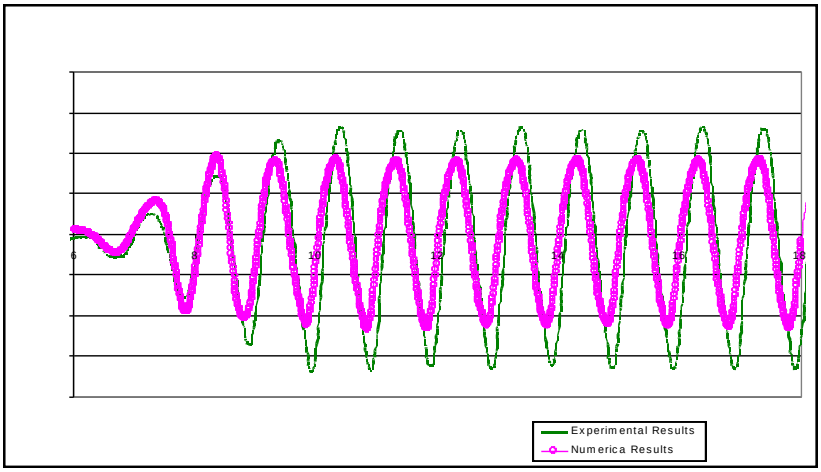

Figure 3.15: Angular displacement of WRASPA against linear waves of 20 mm amplitude.

Table 3.4 shows a comparison between the standard deviation of the time history of the experimental and simulated displacement angle.

Table: 3.4 Comparison of Stdev Value of Displacement Angle

Wave Amp. (mm)	Experimental Pitch Motion (rad)	Simulated Pitch Motion (rad)	Error %
10	0.221124	0.219683	0.65
20	0.321596	0.262261	18.45

3.2.4 Characterization Test

During these tests the device was held still against the same incident waves as the previous test and the torque (to maintain stationary) was computed using different wave amplitudes. This gives a measure of the output power (power = angular frequency x torque). The results of this test (for RHM2) were given against experimental results in Figure 3.16. To begin to optimize power output, two different collector body shapes, RHM2 and RHM3 (Figure 3.17) were tested numerically using the characterization tests. The torques from both shapes was plotted over time (Figure 3.18).

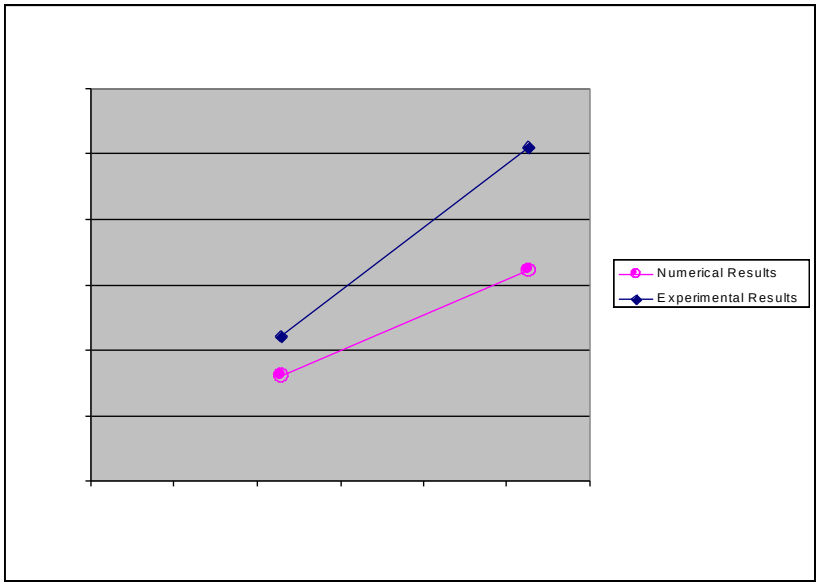

Figure 3.16: Torque (Nm) v Wave amplitude (mm) for fixed collector

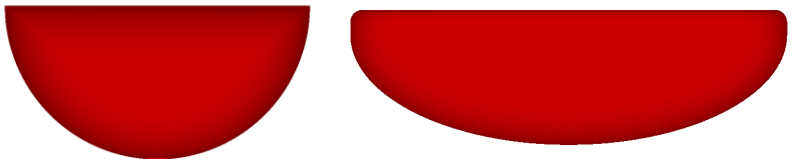

(a) (b)

Figure 3.17: Front view of two collector shapes (a) RHM2 (b) RHM3

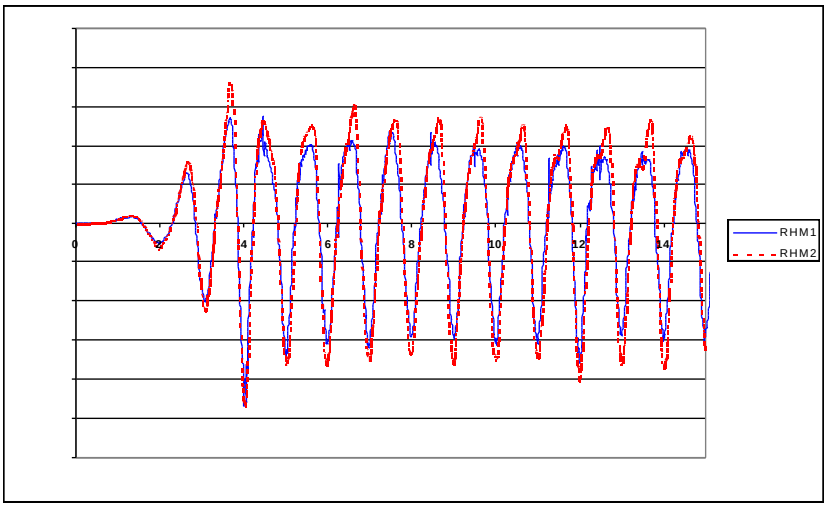

Figure 3.18: Numerical results of time history of torque for shapes RHM2 and RHM3 from the characterization tests.

A visual comparison of experimental and numerical setup was given in Figure 3. 19.

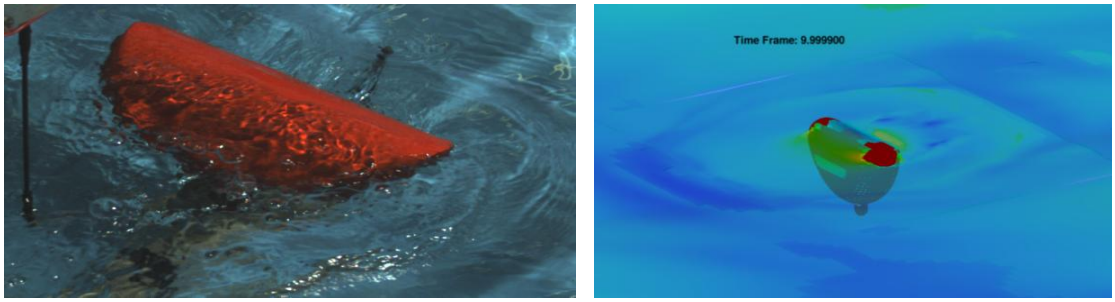

(a) (b)

Figure 3.19: WRASPA (RHM2) in action (a) Experimental wave tank (b) Numerical wave tank

The numerically modelled incident waves and resulting surging response of the WRASPA device at various instants is shown in Figure 3.20.

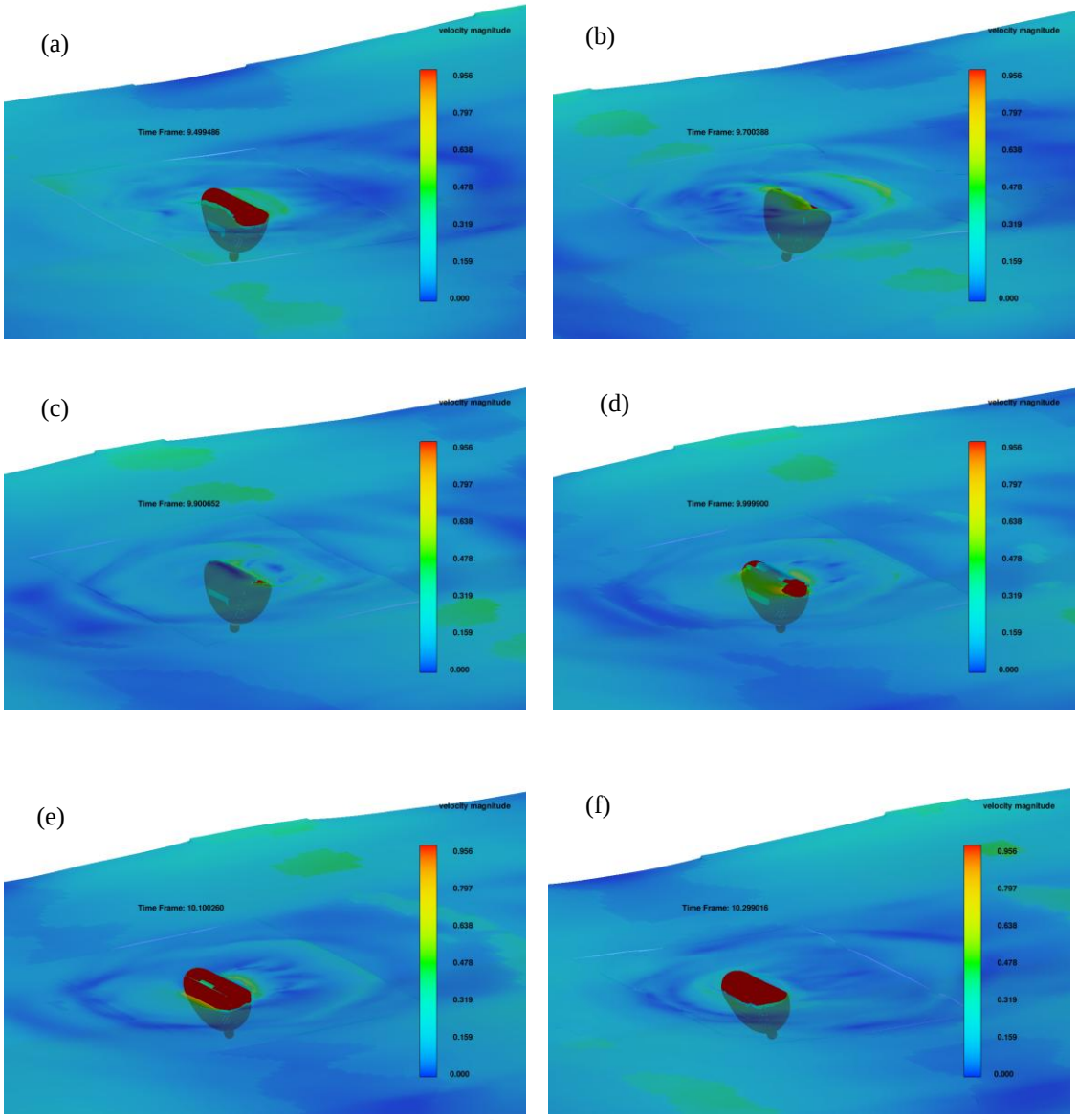

Figure 3.20: Wave interaction with WRASPA (RHM2) at various t seconds (a) t=9.50 (b) t=9.70 (c) t=9.90 (d) t=9.99 (e) t=10.10 (f) t=10.30.

3.3 Achievements / Output (Papers)

- Device in surge modelled successfully. This relates to ID-3 of the project Gantt chart (Appendix 3A).
- Damped oscillations of the device modelled successfully, computing its natural frequency. This relates to ID-3 of initial project Gantt chart.
- Shape optimization modelled for two set of collector shapes. Relates to ID-5 of initial project Gantt chart.

MMU has submitted three conference papers, presenting the combined work of both project partners.

OMAE 2009
ICCEP2009
EWTEC2009

Details of these papers are as follows:

[3.1] Bhinder M.A., Mingham C.G., Causon D.M., Rahmati M.T., Aggidis G.A. and Chaplin R.V. " A joint numerical and experimental study of a surging point absorbing wave energy converter (WRASPA)", *Proceedings of ASME 28th International Conference on Ocean, Offshore and Arctic Engineering*, OMAE2009-79392. Appendix (C).

[3.2] `Bhinder M.A., Mingham C.G., Causon D.M., Rahmati M.T., Aggidis G.A. and Chaplin R.V. " Numerical and experimental study of a point absorber wave energy converter in regular waves", ICCEP 2009. Appendix (D).

[3.3] Bhinder M.A., Mingham C.G., Causon D.M., Rahmati M.T., Aggidis G.A. and Chaplin R.V. " Numerical Modelling of a wave energy converter", EWTEC 2009. Appendix (E).

3.4 Future Work

- Non-linear wave modelling for real sea scenario
- Controlled motion modelling
- Further shapes to be tested for power optimization
- Modelling of larger scale models to predict power output for larger scales.
- Modelling of more than one device (array of devices)

4. APPENDICES

APPENDIX A - Patent

Extrac from Patent Application 20080616 – “Hammerhead”

Drawings

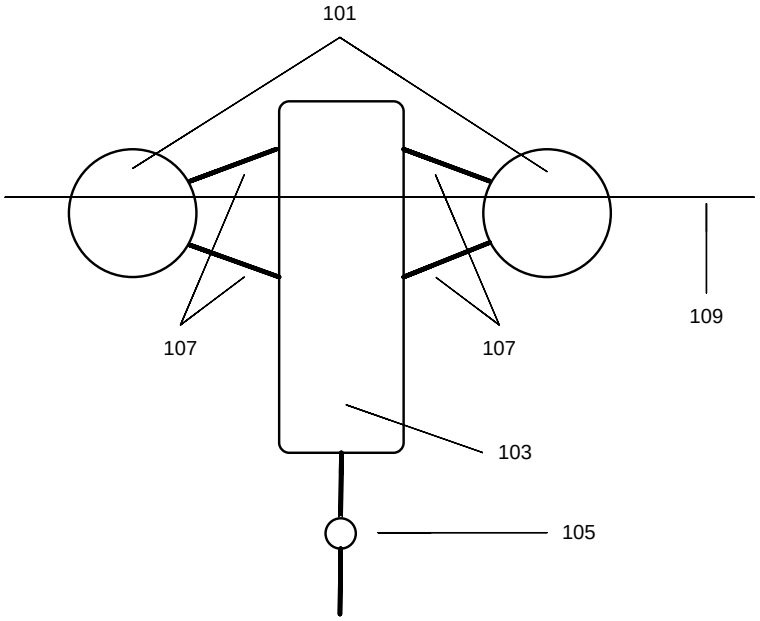

Figure 1

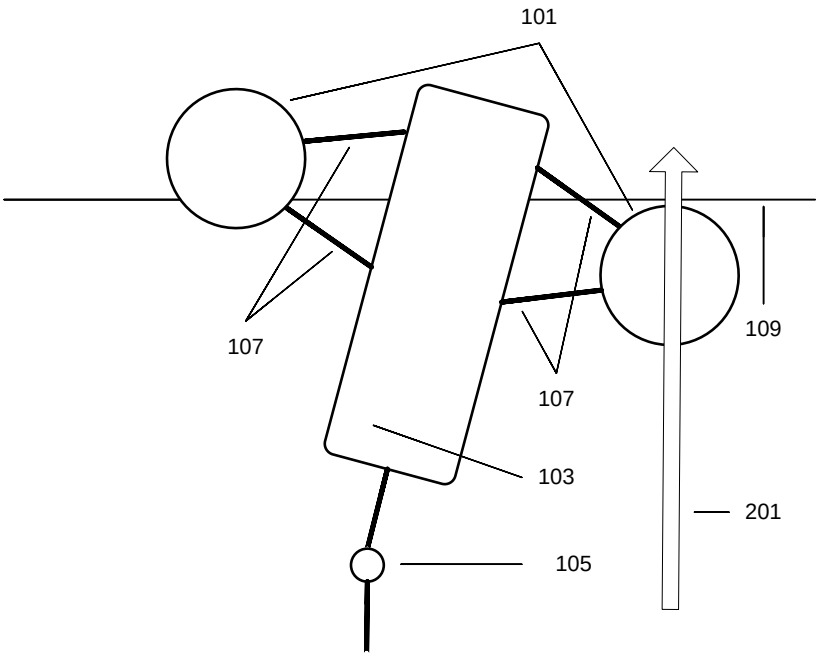

Figure 2

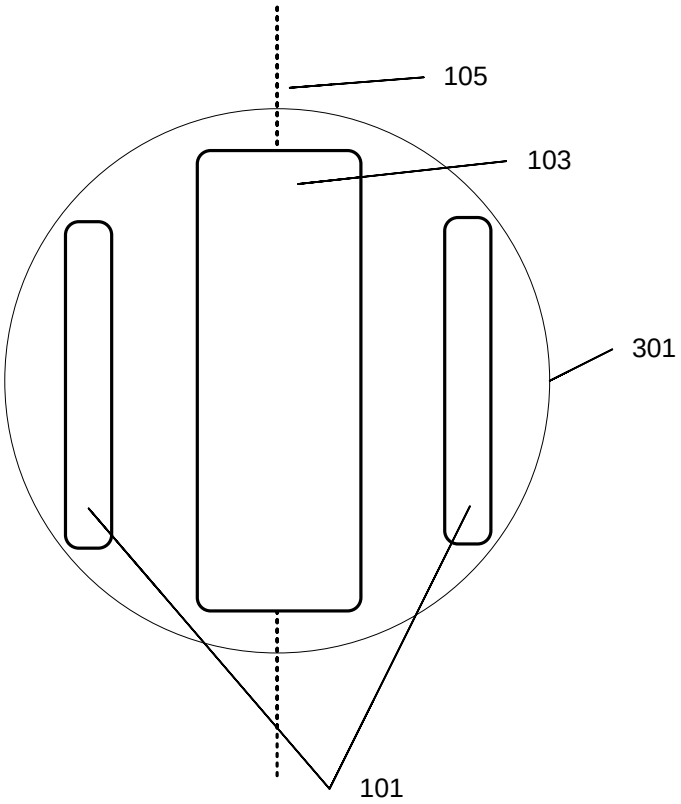

Figure 3 (plan view)

CLAIMS

A device for extraction of energy from moving water, comprising a collector mounted substantially perpendicular to the direction of movement of water and able to pivot about a substantially horizontal axis below it, and at least one buoyant body rigidly attached fore and/or aft of the collector at a distance from the collector, the buoyant body being at or near the undisturbed water surface; and the motion of the device about the axis providing means for power extraction

A device according to Claim 1 where the connections linking the one or more buoyant bodies to the collector incorporate devices able to alter the overall device geometry during operation, including without limitation levers and/or actuators including hydraulic actuators

ABSTRACT

IMPROVED WAVE ENERGY DEVICE

The invention is a wave energy converter of the “bottom-hinged plate” type, improved over previous designs by incorporating at least one buoyancy body and thus giving increased rotational restoring torque and decreased rotational inertia. This serves to increase the converter’s power by allowing larger devices to be built with desirable resonance properties. Additionally, altering the geometry of the buoyancy bodies during operation allows real-time tuning to prevailing sea conditions and optimisation of power extraction

.

APPENDIX B - Website

http://www.lancs.ac.uk/fas/engineering/lureg/group_research/